GEOLOGICAL SURVEY OF CANADA
OPEN FILE 7421

3D Magnetic Inversion of Mineral Prospects in the Great Bear Magmatic Zone, Northwest Territories

N. Hayward

2013

Natural Resources Canada | Ressources naturelles Canada

Canada

GEOLOGICAL SURVEY OF CANADA
OPEN FILE 7421

3D Magnetic Inversion of Mineral Prospects in the Great Bear Magmatic Zone, Northwest Territories

N. Hayward

Geological Survey of Canada, 1500-605 Robson Street, Vancouver, BC

2013

doi:10.4095/292662

This publication is available for free download through GEOSCAN (http://geoscan.ess.nrcan.gc.ca/)

Recommended citation
Hayward, N., 2013. 3D Magnetic Inversion of Mineral Prospects in the Great Bear Magmatic Zone, Northwest Territories; Geological Survey of Canada, Open File 7421. doi:10.4095/292662

Publications in this series have not been edited; they are released as submitted by the author.

Abstract

The Great Bear magmatic zone is a Paleoproterozoic continental magmatic arc in the Northwest Territories, Canada. Interpretation of aeromagnetic data shows the region to be associated with high-amplitude magnetic anomalies which are related to zones of iron oxide-alkali-altered rocks and polymetallic iron oxide-copper-gold deposits and prospects.

Iron oxide-alkali-altered rocks in the field may be obscured by surficial cover and lakes, and surface exposures may not be representative of the extent and intensity of alteration. Therefore geophysical techniques are employed to investigate regional prospects across the variably exposed and inaccessible terrain. Three-dimensional magnetic inversion models are constructed for twelve of the prospects and deposits in order to investigate the scale, geometry and magnetic susceptibility of their highly magnetite-altered zones. The choice of model locations was guided by known mineral prospects, targets resulting from prior two-dimensional geophysical methods, and the extent of the associated magnetic anomalies.

Introduction

The Great Bear magmatic zone (GBMZ) is a Paleoproterozoic continental magmatic arc, populated by polymetallic iron oxide-copper-gold (IOCG) deposits and prospects (Fig. 1) (NORMIN database, NTGO 2012; Mumin et al., 2007, 2010; Corriveau et al., 2010a,b). Details of the distribution and character of IOCG prospects, across what is a large area (> 50,000 km^2) of inaccessible terrain, have been provided through the compilation (Hayward and Oneschuk, 2011) and interpretation of aeromagnetic data (Fig. 2), geophysical targeting (Fig. 3) (Hayward et al., 2013), and the application of an alteration vector-to-mineralisation model (Corriveau et al., 2010a, b) to geological observations.

IOCG deposits may include a broad range of magnetite-, magnetite-to-hematite and hematite-group deposits, and affiliated deposits such as iron oxide-apatite and albitite-hosted uranium deposits (Hitzman et al., 1992; Williams et al., 2005; Corriveau et al., 2010a; Williams, 2010a; Porter, 2010a; Groves et al., 2010). They may be formed during the interaction of tectonically driven (Oliver et al., 2008; Porter, 2010a; Skirrow, 2010) iron oxide alkali-altered (IOAA) hydrothermal systems with host rocks, including uranium-rich hosts and breccia zones (Jébrak, 2010). Major changes in the mineralogy and physical properties of the rocks result from the intense alteration (Sandrin et al., 2009; Corriveau et al., 2010a; Montreuil et al., 2013, in press). Collectively magnetite, magnetite-amphibole, magnetite-K-feldspar, biotite-magnetite, and hematite (with intense retrogression to magnetite) alteration may lead to high-amplitude magnetic anomalies due to an increase in the magnetic susceptibility and remanent magnetisation (Belperio et al., 2007; Williams, 2010b).

In the Mount Isa Block and Gawler Craton, Australia; west Kiruna, Sweden; and NICO and Echo Bay, Canada (Webb and Rowston, 1995; Goad et al., 2000b; Hitzman, 2000; Smith, 2002; Cooper Minerals, 2007; Sandrin et al., 2007; Williams, 2010b; Hayward et al., 2013), IOAA alteration and IOCG deposits are commonly associated with near-offset or coincident magnetic and gravity anomalies. At the Prominent Hill and Carrapateena deposits (Belperio et al., 2007; Porter, 2010b), IOCG mineralisation occurs at the transition from magnetite-rich to hematite-rich potassic alteration, that may be reflected in the transition between magnetic and gravity highs.

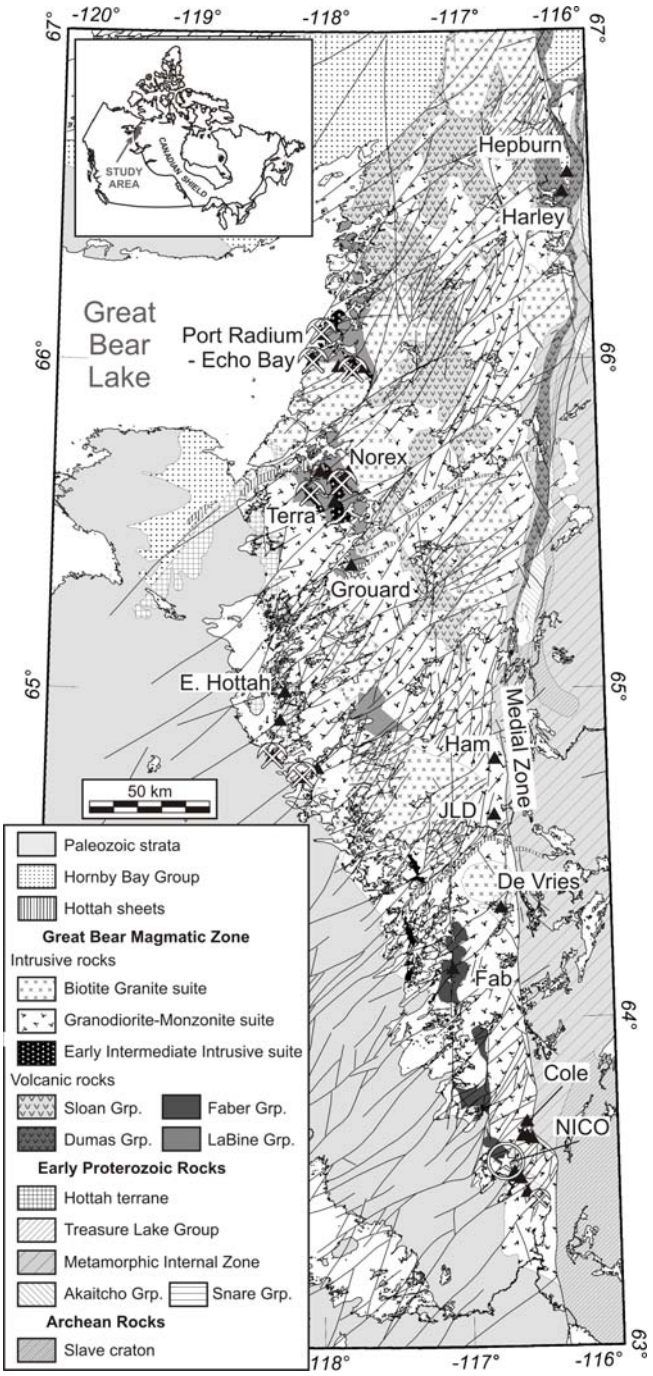

Figure 1: Location and regional geology of the GBMZ. Geology simplified from Hildebrand (2011), Hoffman and Hall (1993), Jackson (2008), and Gandhi et al. (2001). Black triangles show selected mineral prospects discussed in the text. Crossed hammers show the location of historical mines. Circled stars show the location of known mineral deposits. NE-striking faults derived from geophysical anomalies under the sedimentary cover to the west of the GBMZ are located on figure although they do not cut across the Paleozoic cover.

Here we apply 3D magnetic inversion (Pilkington, 2009) to the investigation of the three-dimensional geometry and susceptibility variation of magnetite alteration zones associated with IOCG and affiliated prospects, which may be obscured by cover or not be accurately represented by their surface exposure.

Geological Setting

The GBMZ (Fig. 1) is a Paleoproterozoic (Andean-type) continental magmatic arc (*ca.* 1.872–1.843 Ga) which forms part of the Wopmay Orogen (1.92-1.84 Ga, Hoffman, 1980). During the Calderian orogeny (*ca.* 1.88 Ga), sedimentary, volcanic and crystalline basement rocks of the Coronation margin were thrust onto the Slave Craton (Cook et al., 1999; Hildebrand at al., 2010a) and associated with the accretion of the Hottah terrane. The GBMZ was intruded into and deposited upon the Hottah terrane and Coronation margin between 1.87 and 1.84 Ga (Hoffman and Bowring, 1984), during eastward subduction of oceanic lithosphere attached to the Fort Simpson terrane (Hildebrand et al., 2010a).

The GBMZ is composed primarily of plutonic rocks of the Granodiorite-monzonite suite (*ca.* 1.86 Ga) (Hoffman and McGlynn, 1977; Hildebrand et al., 1987), which are bounded to the east by the Medial zone (Fig. 1). These were preceded by the Early intermediate intrusive suite (*ca.* 1.872 Ga, Davis et al., 2011) diorite sub-volcanic laccoliths in the north and felsic porphyries in the south intrude their own volcanic and volcaniclastic eruptive sequences respectively of the LaBine Group in the north and Faber Group in the south (Goad et al., 2000a, b; Gandhi et al., 2001; Hildebrand et al., 2010b; Davis et al., 2011). Some of the early volcanic rocks are overlain by volcanic and sedimentary rocks of the Sloan Group, which is contemporaneous with the intrusions of the Granodiorite-monzonite suite and some porphyry intrusions.

IOAA alteration and breccia systems are associated with IOCG and affiliated mineralisation and are either developed 1) within the Treasure Lake Group metasedimentary rocks and other components of the Hottah terrane below their unconformity with overlying volcanic rocks of the Faber Group such as in the NICO deposit, or within the internal unconformity of the Hottah terrane such as at the East Hottah prospect; 2) within the Faber Group, or 3) within the LaBine Group as at Port Radium-Echo Bay, where IOCG and iron oxide-apatite mineralisation (*ca.* 1.873 – >1.866 Davis et al. 2011) was coeval with emplacement of diorite intrusions of the Early intermediate intrusive suite (Hildebrand, 1986; Goad et al., 2000a, b; Corriveau et al., 2010b; Mumin et al., 2007, 2010).

Rocks of the GBMZ were gently folded at *ca.* 1.86-1.85 Ga (Hildebrand et al., 1987), followed by the emplacement of Rapakivi syenogranite intrusions of the Biotite granite suite (*ca.* 1.858 – 1.843 Ga, Bowring, 1984; Gandhi et al., 2001). The GBMZ was then cut by extensive NE-striking, right-lateral faults (Tirrul, 1984).

Mafic dyke swarms (Buchan and Ernst, 2004; Buchan et al., 2010) later intruded the GBMZ. The WNW-ESE trending Cleaver dykes (*ca.* 1740 Ma) crosscut the GBMZ north of 65° N, but do not extend east of the Medial zone (Irving et al., 2004). Younger intrusions of the Mackenzie (*ca.* 1267 Ma), Gunbarrel-Hottah (*ca.* 767 Ma) and Franklin (*ca.* 728-716 Ma) dyke swarms are less pervasive and tend to exploit the relict structural fabric of the arc.

The GBMZ is unconformably overlain by Paleozoic carbonates and the cryptic Desert Lake Paleoproterozoic sequence to the west and by mid-Proterozoic sedimentary rocks of the Hornby Bay basin to the northwest (Bleeker et al., 2007).

Aeromagnetic data

Aeromagnetic data for this study were compiled from publically available data (Hayward and Oneschuk, 2011; Mazenod Lake: Hetu et al., 1994; Lac la Marte and Southwestern Wopmay Orogen: NTGO, 2006, 2008; Northern GBMZ: Harvey et al., 2009; Hottah Lake: Kiss and Coyle, 2011), in combination with proprietary high-resolution data from NICO (Pritchard, 1995), Hepburn Lake (acquired by private sector under contract for Diamonds North Resources Ltd.) and Lever Lake (acquired by private sector under contract for Yankee Hat Minerals Ltd.). Individual survey parameters are given in Table 1.

Table 1: Acquisition parameters for aeromagnetic surveys in the Great Bear magmatic zone.

Survey	Year	Line Spacing	Survey Height
Northern Great Bear magmatic zone	2009	400 m	125 m
Southwestern Wopmay Orogen	2007	400 m	125 m
Hottah Lake	2011	400 m	150 m
Lac la Martre	2006	400 m	150 m
Mazenod Lake	1993	500 m	120 m
Hepburn Lake	2007	100 m	25 m
NICO	1995	100 m	100 m
Lever Lake	2005	250 m	50 m

Residual total field magnetic anomalies have a background of ~50-300 nT (Fig. 2) primarily associated with the Granodiorite-monzonite suite plutons and Sloan Group volcanic rocks which dominate the area (Fig. 1). The highest amplitude anomalies (~2000-5000 nT) are commonly associated with hydrothermally altered, and sometimes mineralised, volcanic rocks of the LaBine and Faber groups (Fig. 1) as well as hydrothermally altered metasedimentary rocks of the Treasure Lake Group. The Rapakivi syenogranite intrusions are associated with some of the lowest magnetic anomalies (approximately -100–150 nT) (Fig. 2).

Faults and giant quartz veins are commonly associated with short wavelength, magnetic lows (Figs. 1 and 2), whereas the dyke swarms (Buchan et al., 2010) are typically associated with linear, relatively short-wavelength magnetic highs (Fig. 2). The Cleaver dykes (Fig. 2) (Irving et al., 2004) are prominent in the aeromagnetic data with short-wavelength (~4 km) linear ESE trending anomalies. Their high magnetic amplitudes (~200-400 nT) may have implications for inversion modelling. Conversely, the Hottah sheets (Fig. 2) have lower amplitude magnetic anomalies (50-100 nT).

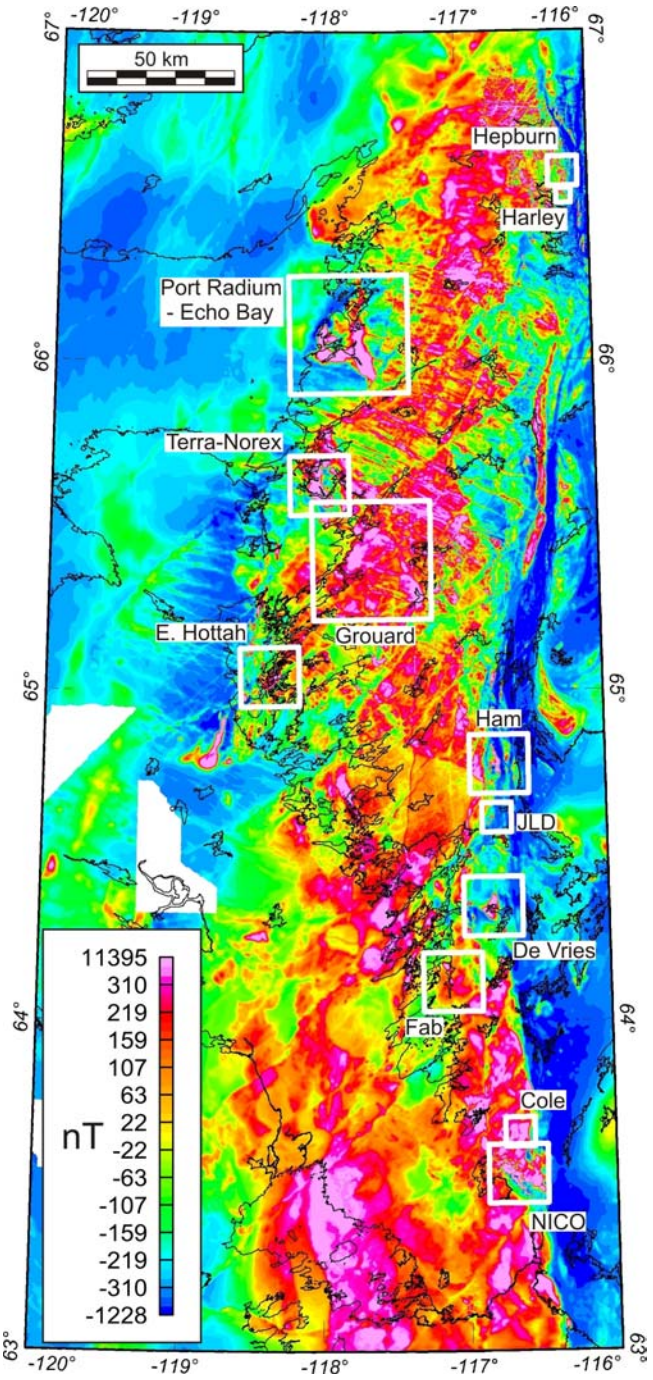

Figure 2: Aeromagnetic compilation of the Great Bear magmatic zone, modified from Hayward and Oneschuk (2011). White boxes show location of 3D magnetic models.

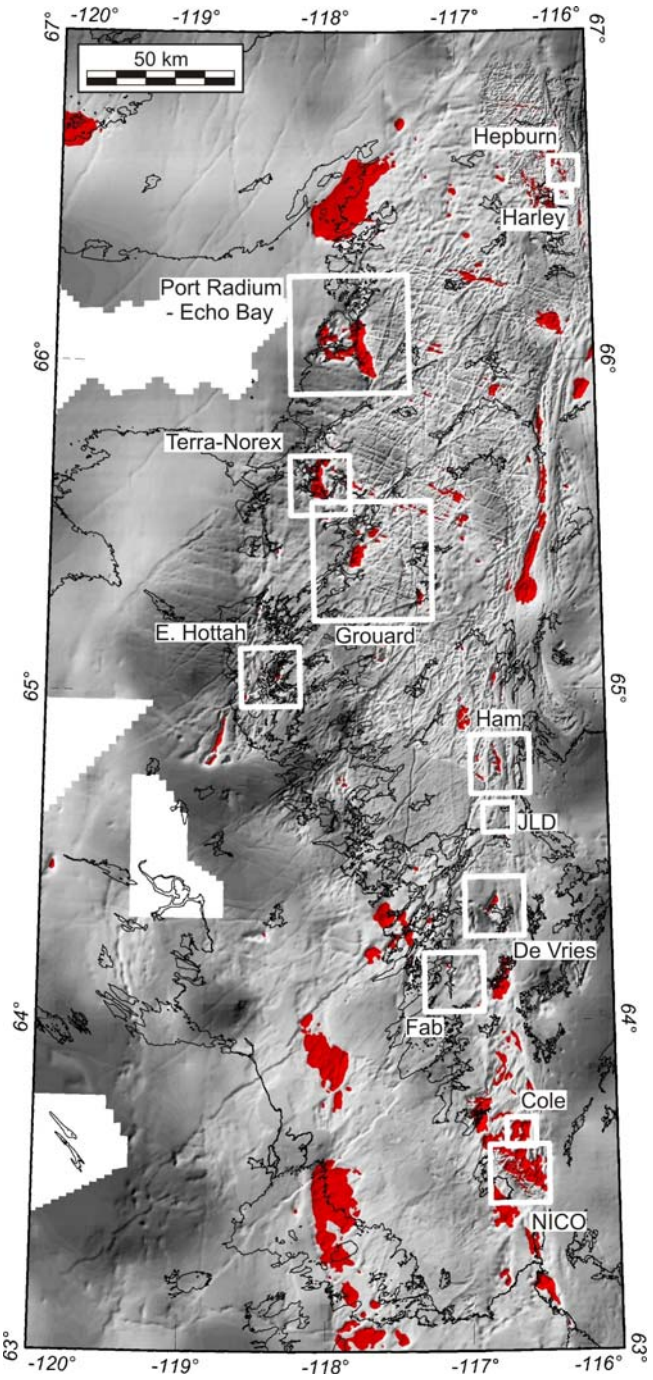

Figure 3: Prospectivity target map of the GBMZ (Hayward et al. 2013). White boxes show location of 3D magnetic models.

3D Inversion Models

The aeromagnetic data were gridded at both 50 and 100 m using a minimum curvature algorithm (Fig. 2). Gridded data were extracted for twelve regions of interest (Fig. 2; Table 2), corresponding to mineral prospects (NTGO, 2012) and geophysically defined targets (Fig. 3). The resolution of the data used to construct the regional grid (Tables 1 and 2) varies geographically and therefore a grid and corresponding model mesh cell size of 50 m were applied in areas covered by high-resolution (100 m line spacing, Table 1) aeromagnetic surveys and a size of 100 m elsewhere. Model dimensions were limited by computer memory and runtime. The largest reasonable models (512 by 512 by 128 cells) had a typical runtime of approximately 1 week on a 3.06 GHz processor and 8 Gb of RAM. The top of each model was defined at the local survey elevation (Table 1) in addition to any applied upward continuation. Only magnetic data for the NICO model, based on older high-resolution data (Table 1), were upward continued (200m) to minimise shallow-sourced perturbations and noise. Aeromagnetic data from the Terra-Norex area (Model 5, Table 2) were pre-filtered with a directional cosine filter (110ºN), and a second model was constructed for Port Radium – Echo Bay (Model 4, Table 2) (directional cosine filter, 105ºN), in order to limit the magnetic signature associated with the Cleaver dykes which are prevalent at these locations (Fig. 2).

Unconstrained inversion of the data from each of the twelve regions (Figs. 4a-15a) was performed using the DSIM3D software package (Pilkington, 2009), with padding cells at the model boundaries to limit edge effects. The predicted magnetic anomalies (Figs. 4c, 5c 6c, 6f, 7c-15c) closely match (see Table 2 for misfit statistics) the primary features of the observed data (Figs. 4b, 5b 6b, 6d, 7b-15b).

Model results are presented graphically as static perspective figures (Figs. 4d, 4e, 5d, 5e, 6f, 6g, 6h, 6i, 7-15d, 7-15e) and interactive 3D PDF files. UBC GIF (University of British Columbia - Geophysical Inversion Facility) format model and mesh files are also supplied which may be viewed using the UBC Meshtools software (http://www.eos.ubc.ca/ubcgif/).

Table 2: 3D magnetic inversion model location and parameters.

Models (North to South)	**Coordinates ($X_{min}/X_{max}/Y_{min}/Y_{max}$) NAD83 UTM 11N**	**Mesh dimensions (X,Y,Z)**	**Grid and model cell size (m)**	**Magnetic data source**	**Upward continuation (m)**	**RMS Error**	**Figure**
(1) Hepburn	531000/540950/7379000/7378950	256, 256, 128	50	Hepburn	0	203	4
(2) Harley	533700/538650/7373200/7378150	128, 128, 64	50	Hepburn	0	95	5
(3) Port Radium-Echo Bay	443000/482900/7309500/7349400	512, 512, 128	100	GBMZ/Canada grid	0	102	6
(4) Port Radium-Echo Bay	443000/482900/7309500/7349400	512, 512, 128	100	GBMZ/Canada grid	0	71	6
(5) Terra-Norex	442300/462200/7268700/7288600	256, 256, 64	100	Canada grid	0	100	7
(6) Grouard	449500/489400/7233000/7272900	512, 512, 128	100	GBMZ/Canada grid	0	90	8
(7) East Hottah	424500/444400/7204200/7224100	256, 256, 128	100	Hottah/GBMZ	0	111	9
(8) Ham	501500/521400/7174000/7193900	256, 256, 64	100	SW Wopmay	0	126	10
(9) JLD	505500/515400/7161000/7170900	128, 128, 64	100	SW Wopmay	0	78	11
(10) DeVries Lake	499000/518900/7126000/7145900	256, 256, 128	100	Canada grid	0	100	12
(11) Fab Lake	485000/504900/7100500/7120400	256, 256, 128	100	Canada grid	0	74	13
(12) Cole Lake	512000/521900/7054700/7064600	128, 128, 64	100	Mazenod	0	190	14
(13) NICO	506200/526150/7035500/7055450	512, 512, 128	50	NICO/Mazenod	200	163	15

Model 1 – Hepburn Lake

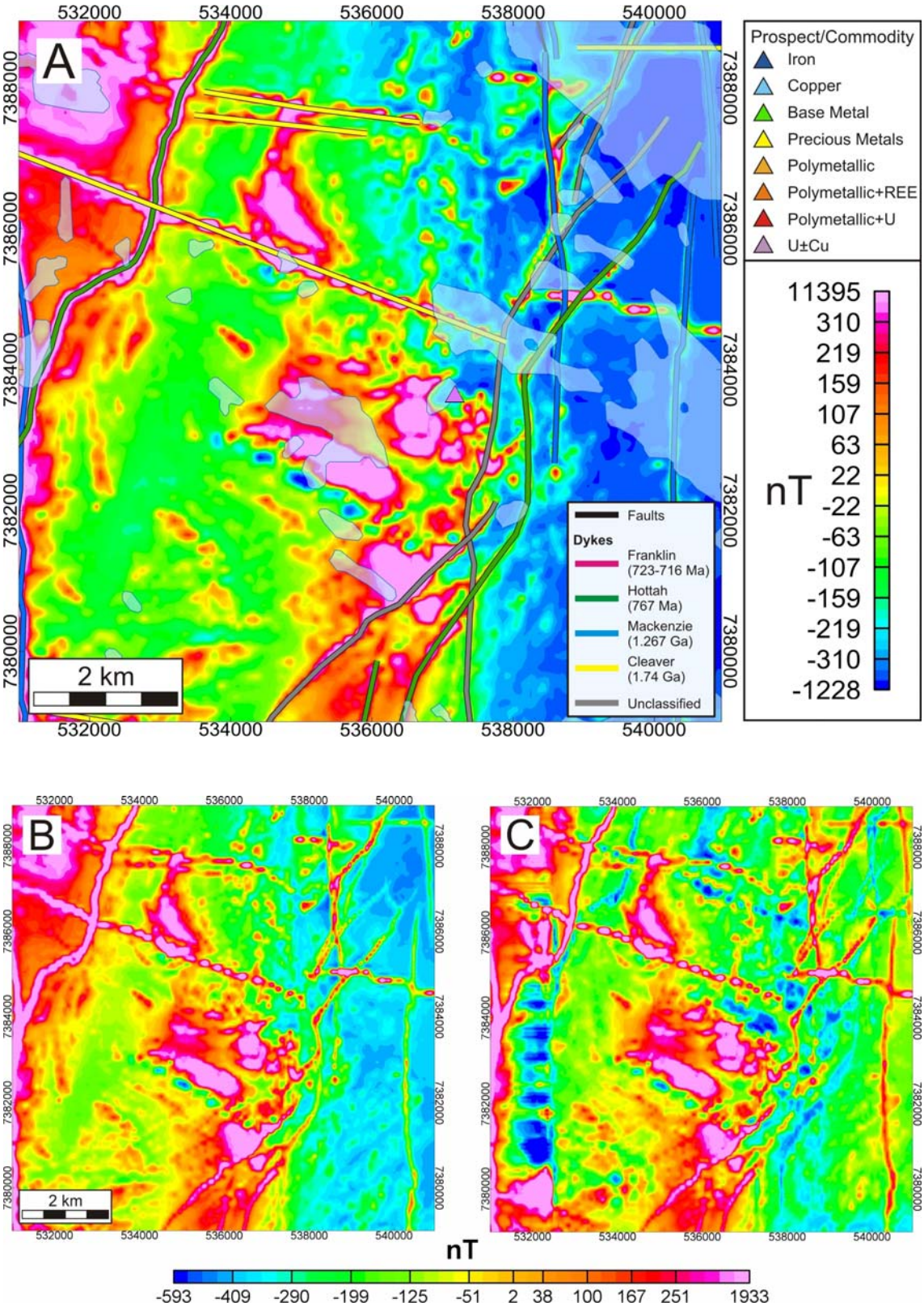

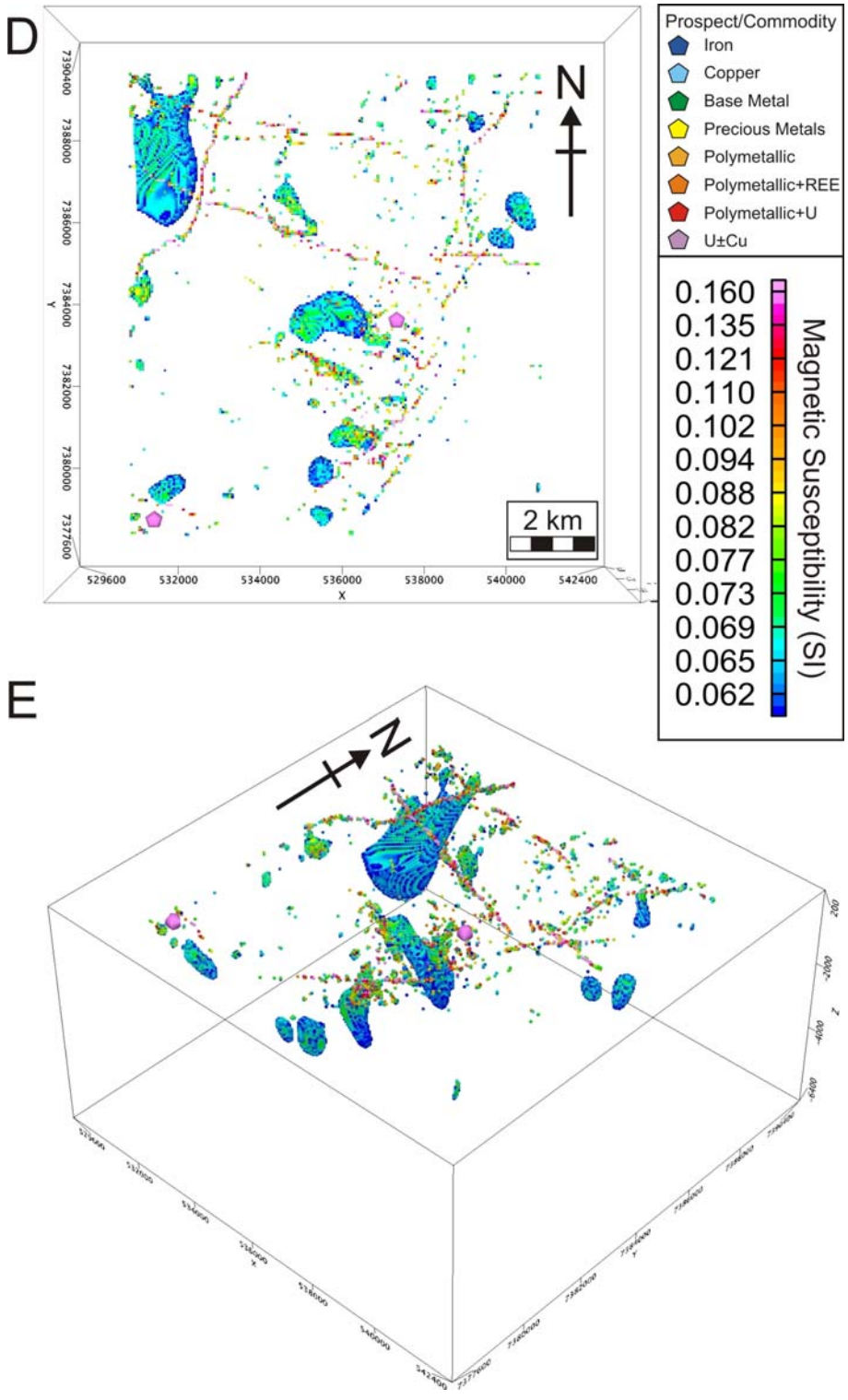

Figure 4: Model 1 - Hepburn Lake area (see Table 2 and Fig. 2 for model location and parameters). a) Interpretation of aeromagnetic data (colour scale as in regional map, Fig. 2). Coloured lines show dykes. Coloured triangles show mineral prospects. b) Observed residual total magnetic field. c) Calculated residual total magnetic field. d) Plan view of 3D magnetic inversion model (magnetic susceptibility window of 0.06 – 0.15 SI). e) Perspective view of 3D magnetic inversion model. Coloured pentagons show mineral prospects.

Model 2 – Harley

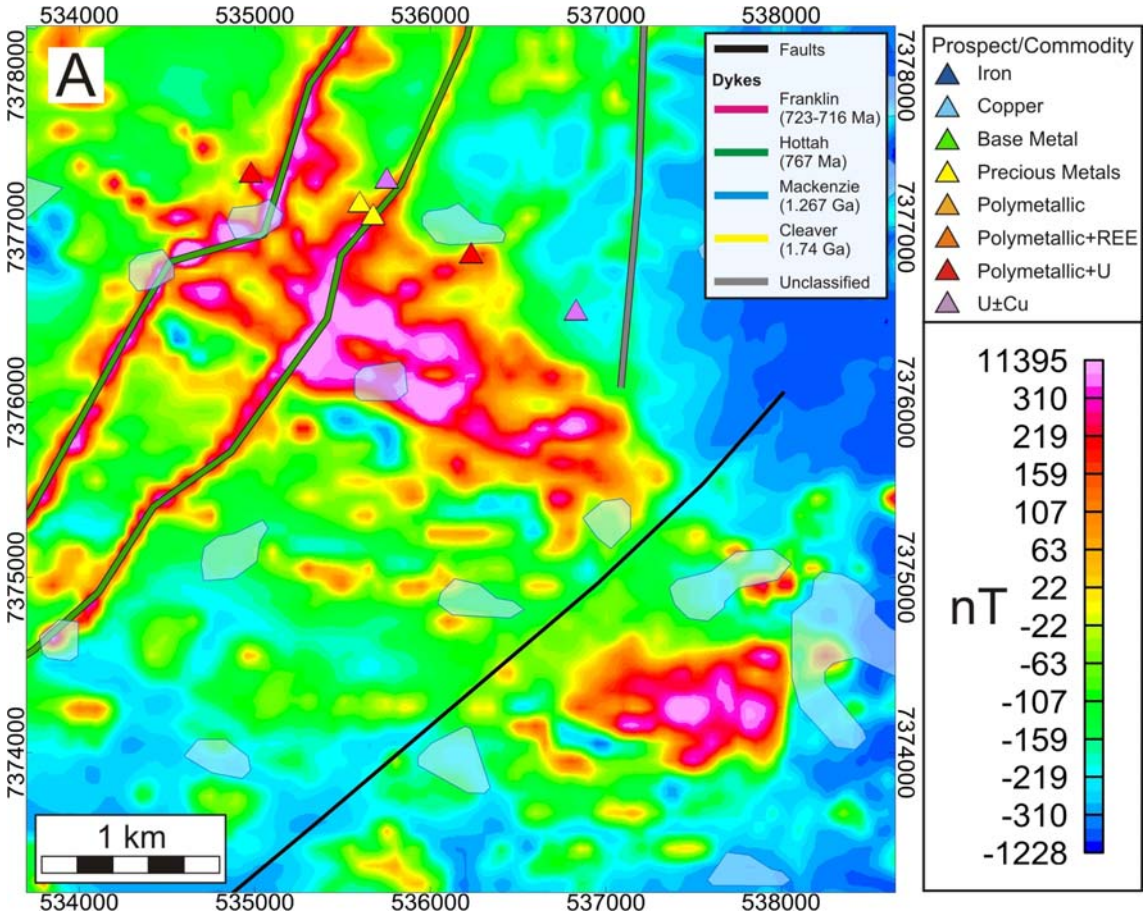

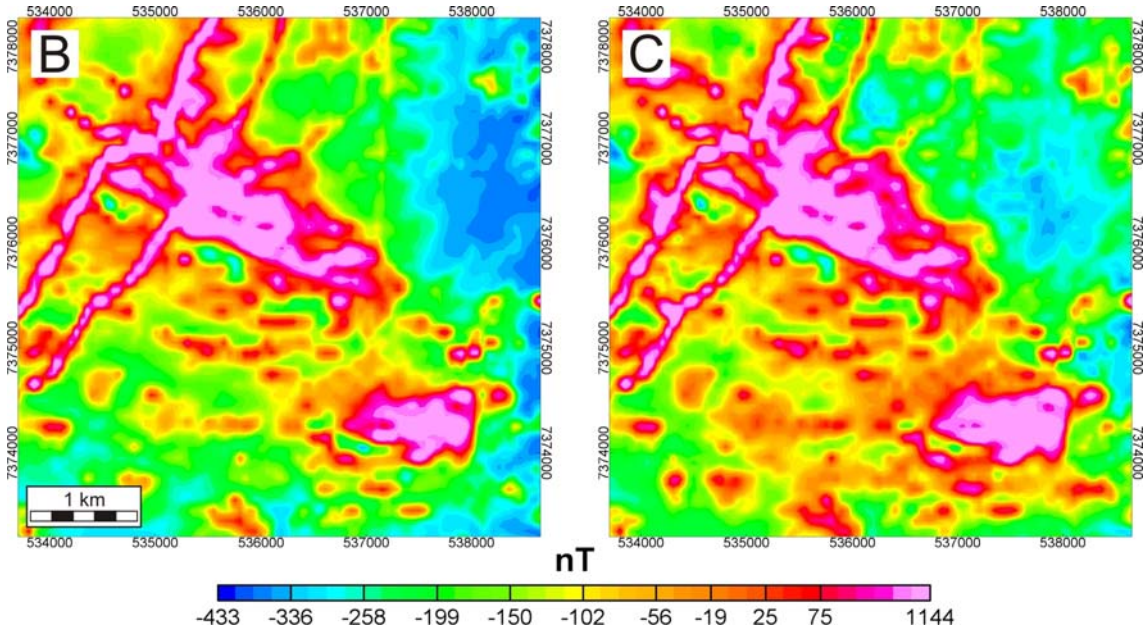

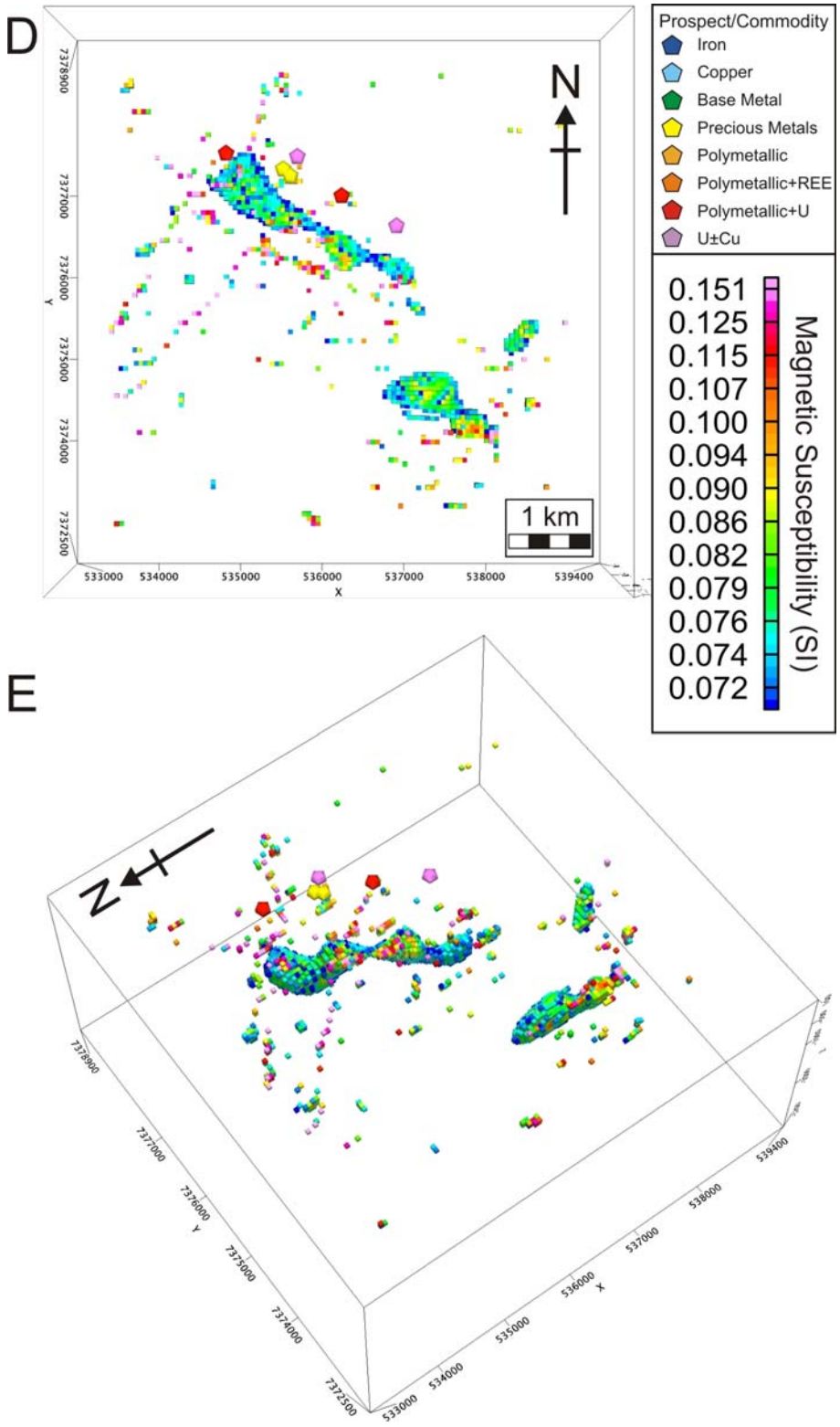

Figure 5: Model 2 – Harley area (see Table 2 and Fig. 2 for model location and parameters). a) Interpretation of aeromagnetic data (colour scale as in regional map, Fig. 2). Coloured lines show dykes. Black lines show faults. Coloured triangles show mineral prospects. b) Observed residual total magnetic field. c) Calculated residual total magnetic field. d) Plan view of 3D magnetic inversion model (magnetic susceptibility window of 0.07 – 0.15 SI). e) Perspective view of 3D magnetic inversion model. Coloured pentagons show mineral prospects.

Models 3 and 4 – Port Radium – Echo Bay

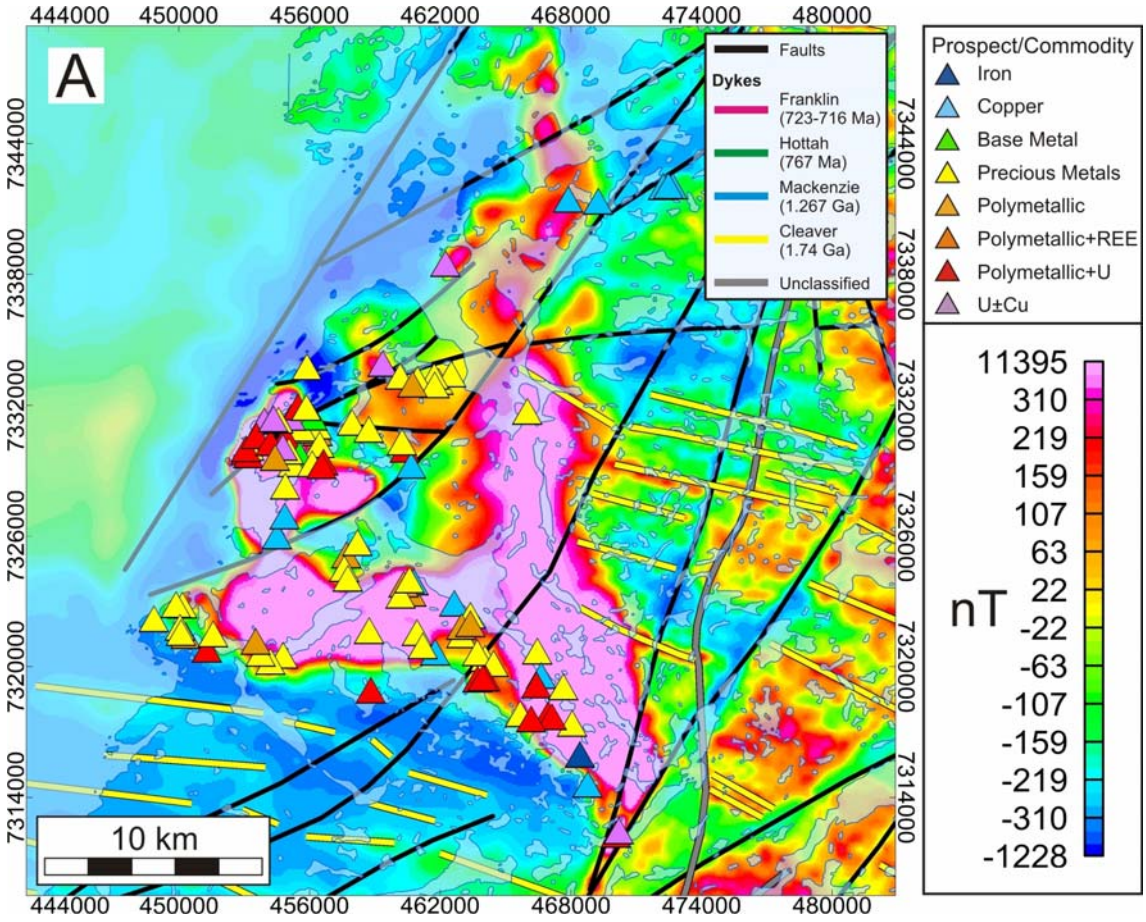

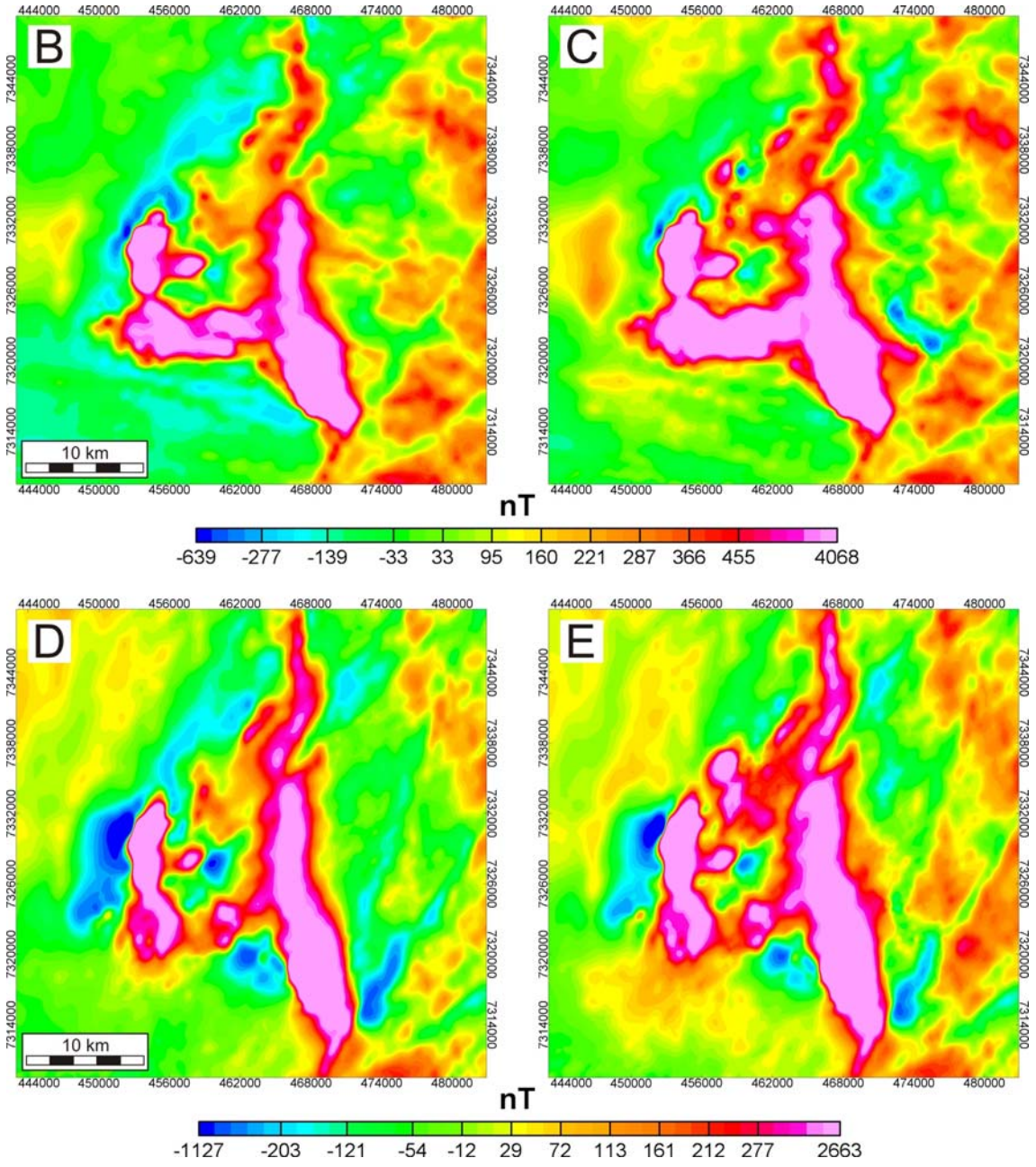
B
C
D
E
444000 450000 456000 462000 468000 474000 480000
7344000 7338000 7332000 7326000 7320000 7314000
10 km
nT
-639 -277 -139 -33 33 95 160 221 287 366 455 4068
-1127 -203 -121 -54 -12 29 72 113 161 212 277 2663

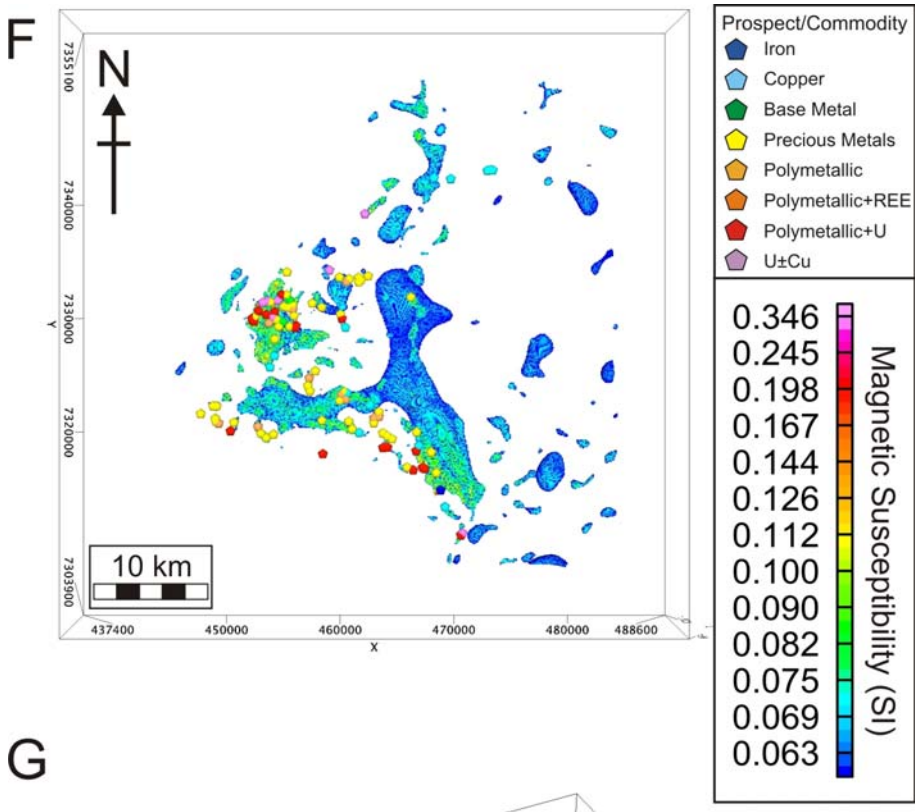
F
N
10 km
7355100
7340000
7330000
7320000
7303900
Y
437400
450000
460000
470000
480000
488600
X
Prospect/Commodity
Iron
Copper
Base Metal
Precious Metals
Polymetallic
Polymetallic+REE
Polymetallic+U
U±Cu
0.346
0.245
0.198
0.167
0.144
0.126
0.112
0.100
0.090
0.082
0.075
0.069
0.063
Magnetic Susceptibility (SI)

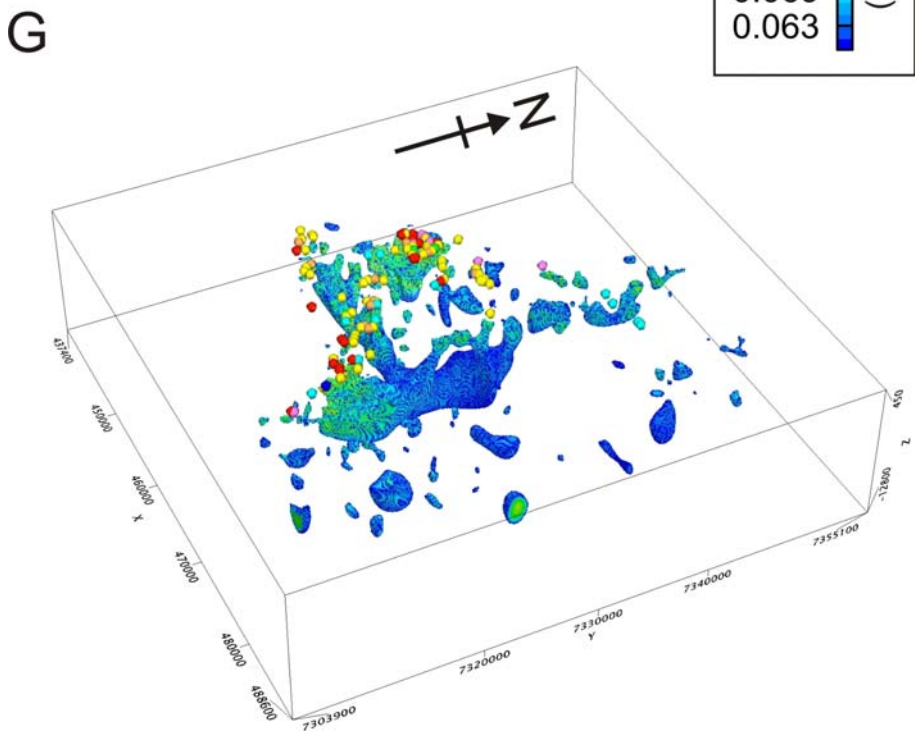
G
Z
437400
450000
460000
X
470000
480000
488600
7303900
7320000
7330000
Y
7340000
7355100
Z

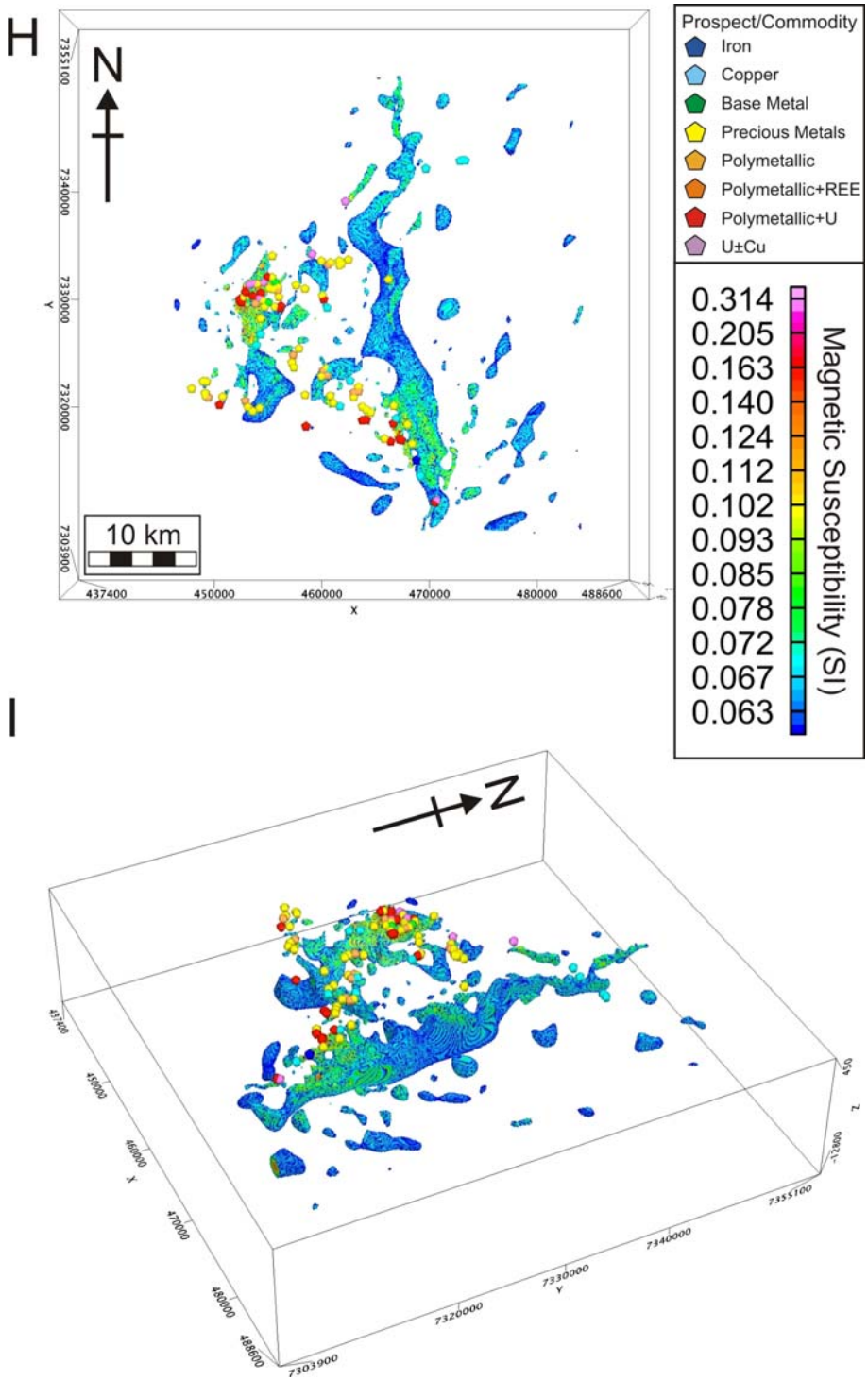

Figure 6: Models 3 and 4 – Port Radium – Echo Bay area (see Table 2 and Fig. 2 for model location and parameters). a) Interpretation of aeromagnetic data (colour scale as in regional map, Fig. 2). Coloured lines show dykes. Black lines show faults. Coloured triangles show mineral prospects. b) Model 3 - Observed residual total magnetic field. c) Model 3 - Calculated residual total magnetic field. d) Model 4 - Observed residual total magnetic field. e) Model 4 - Calculated residual total magnetic field. f) Model 3 - Plan view of 3D magnetic inversion model (magnetic susceptibility window of 0.06 – 0.15 SI). g) Model 3 - Perspective view of 3D magnetic inversion model. h) Model 4 - Plan view of 3D magnetic inversion model (magnetic susceptibility window of 0.06 – 0.15 SI). i) Model 4 - Perspective view of 3D magnetic inversion model. Coloured pentagons show mineral prospects.

Model 5 – Terra-Norex

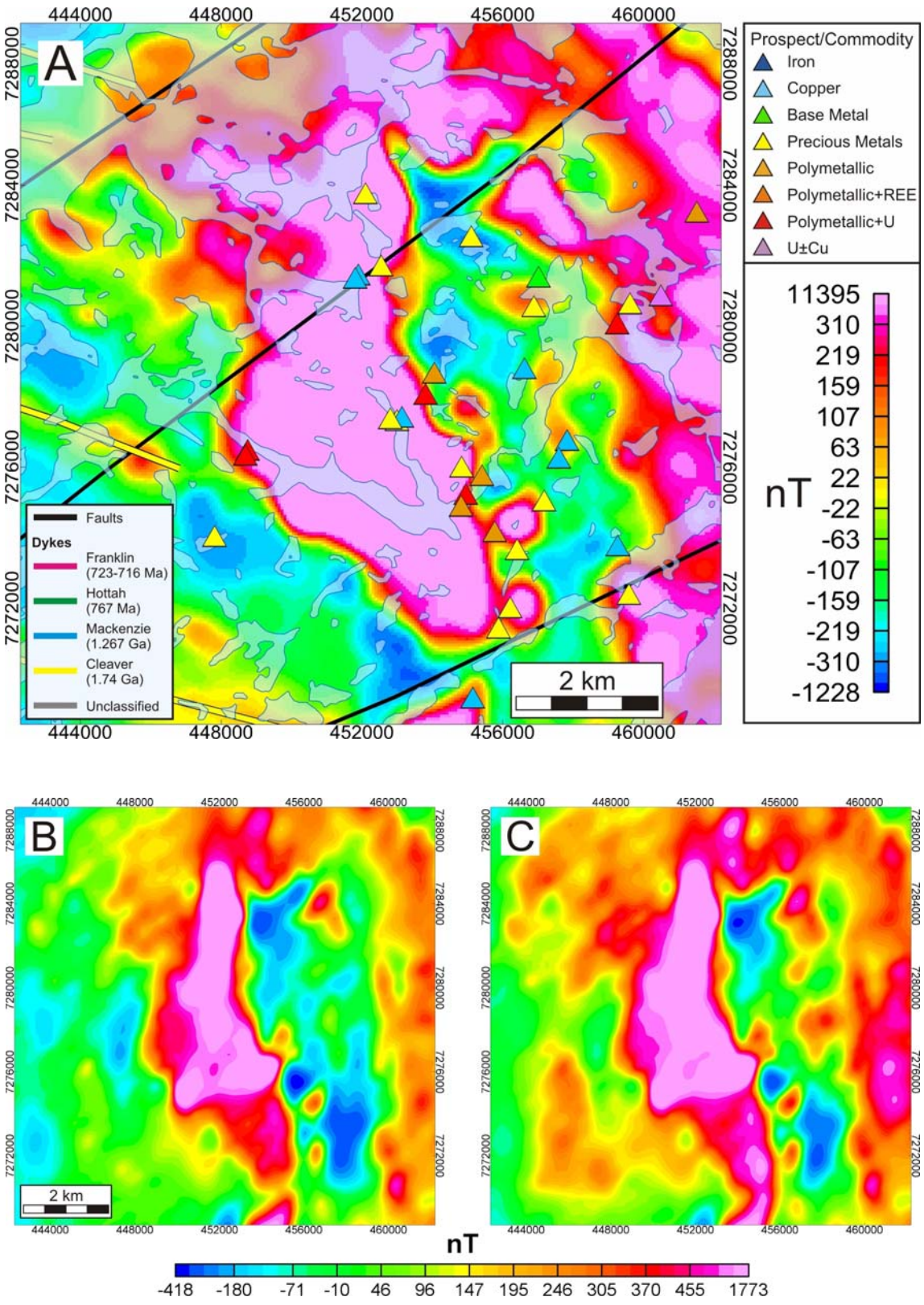

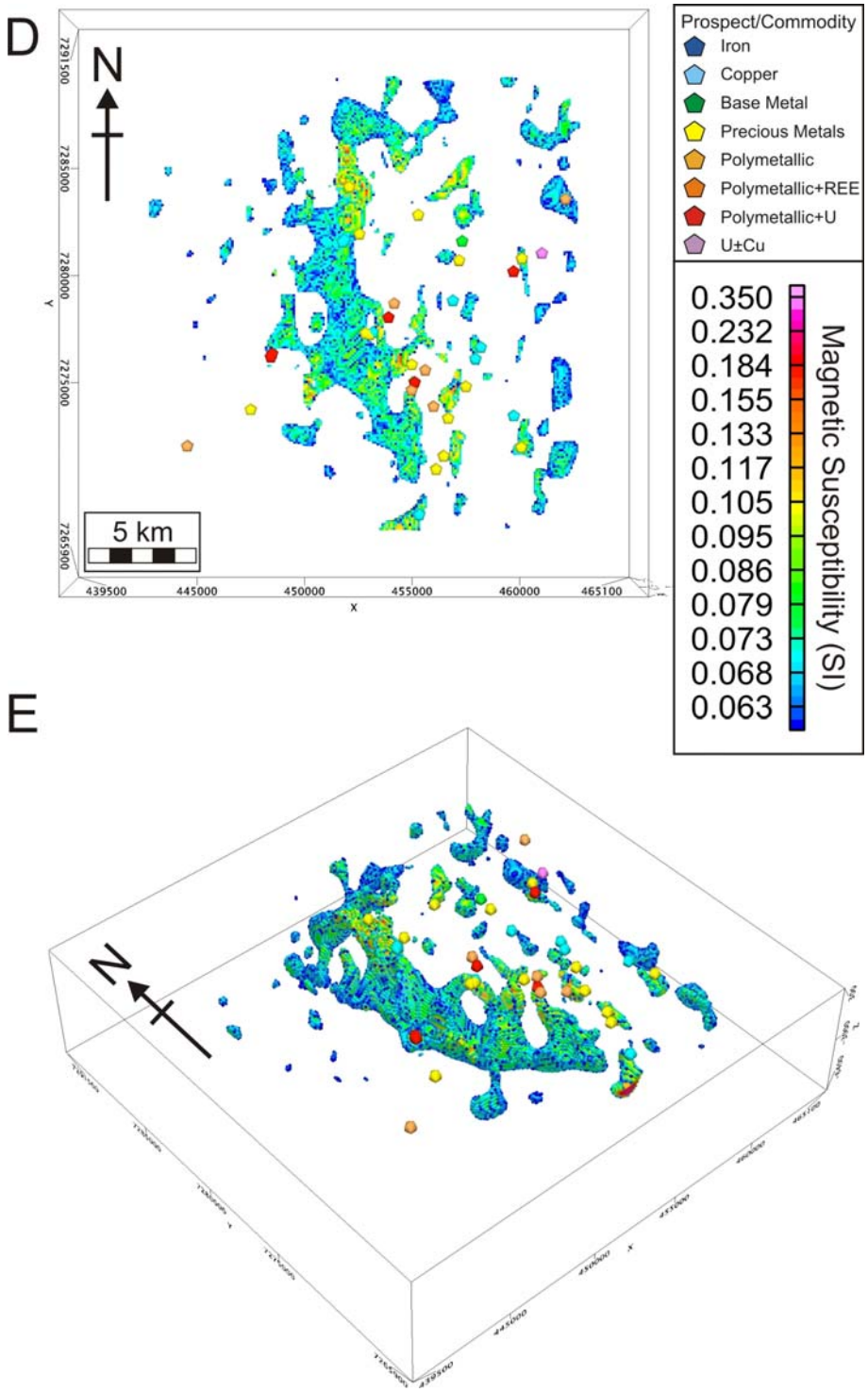

Figure 7: Model 5 – Terra-Norex area (see Table 2 and Fig. 2 for model location and parameters). a) Interpretation of aeromagnetic data (colour scale as in regional map, Fig. 2). Coloured lines show dykes. Black lines show faults. Coloured triangles show mineral prospects. b) Observed residual total magnetic field. c) Calculated residual total magnetic field. d) Plan view of 3D magnetic inversion model (magnetic susceptibility window of 0.06 – 0.15 SI). e) Perspective view of 3D magnetic inversion model. Coloured pentagons show mineral prospects.

Model 6 – Grouard

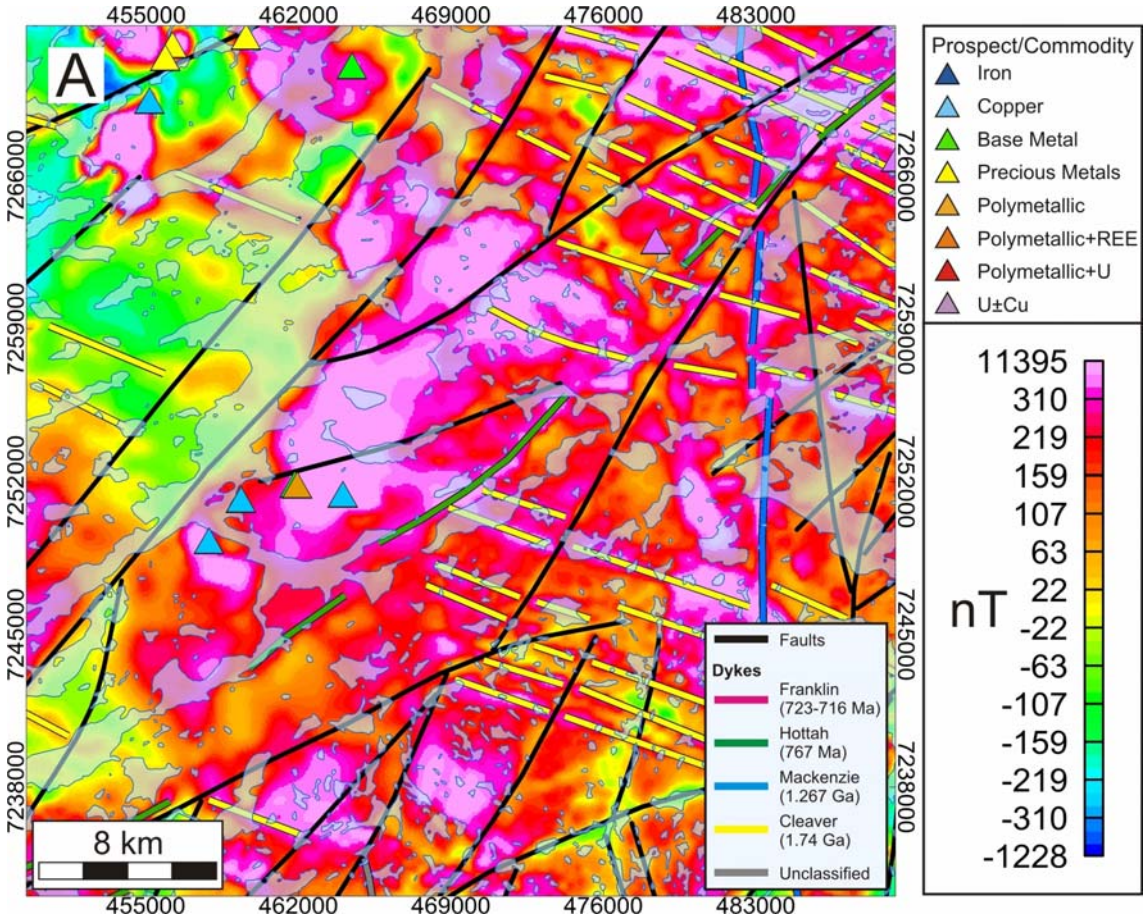

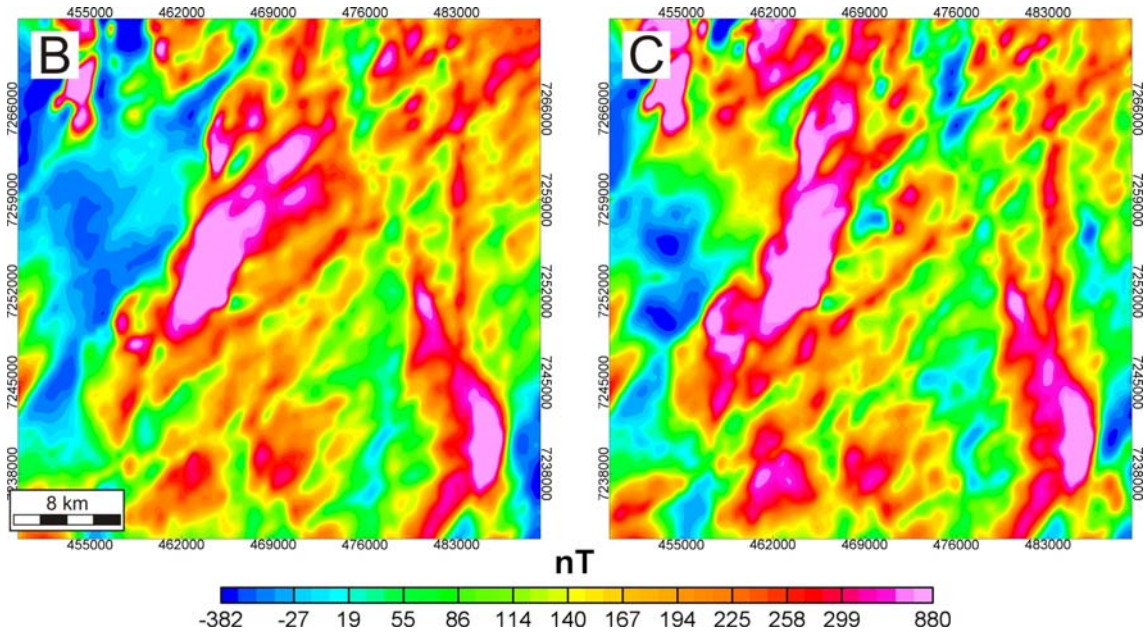

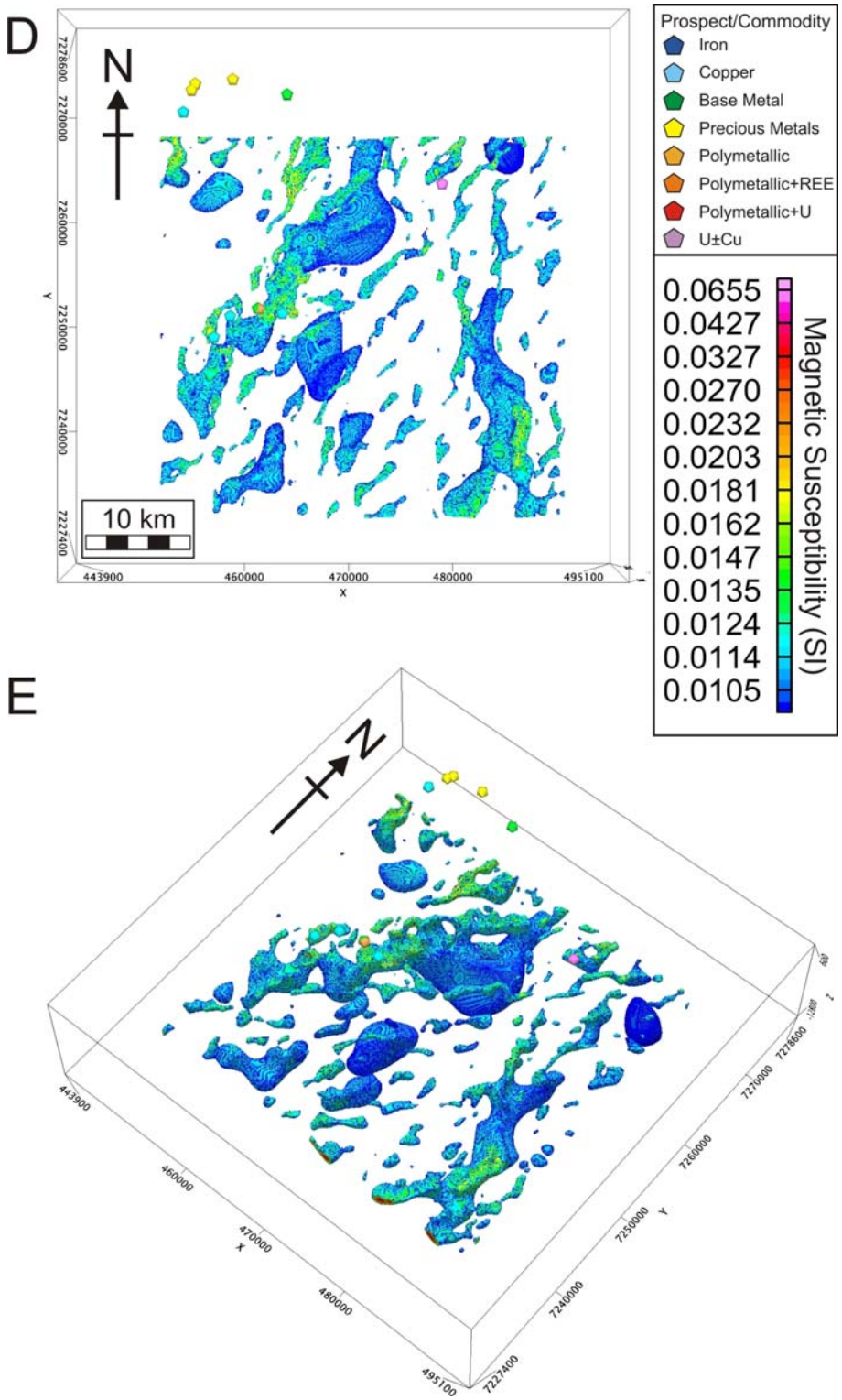

Figure 8: Model 6 - Grouard area (see Table 2 and Fig. 2 for model location and parameters). a) Interpretation of aeromagnetic data (colour scale as in regional map, Fig. 2). Coloured lines show dykes. Black lines show faults. Coloured triangles show mineral prospects. b) Observed residual total magnetic field. c) Calculated residual total magnetic field. d) Plan view of 3D magnetic inversion model (magnetic susceptibility window of 0.01 – 0.04 SI). e) Perspective view of 3D magnetic inversion model. Coloured pentagons show mineral prospects.

Model 7 – East Hottah

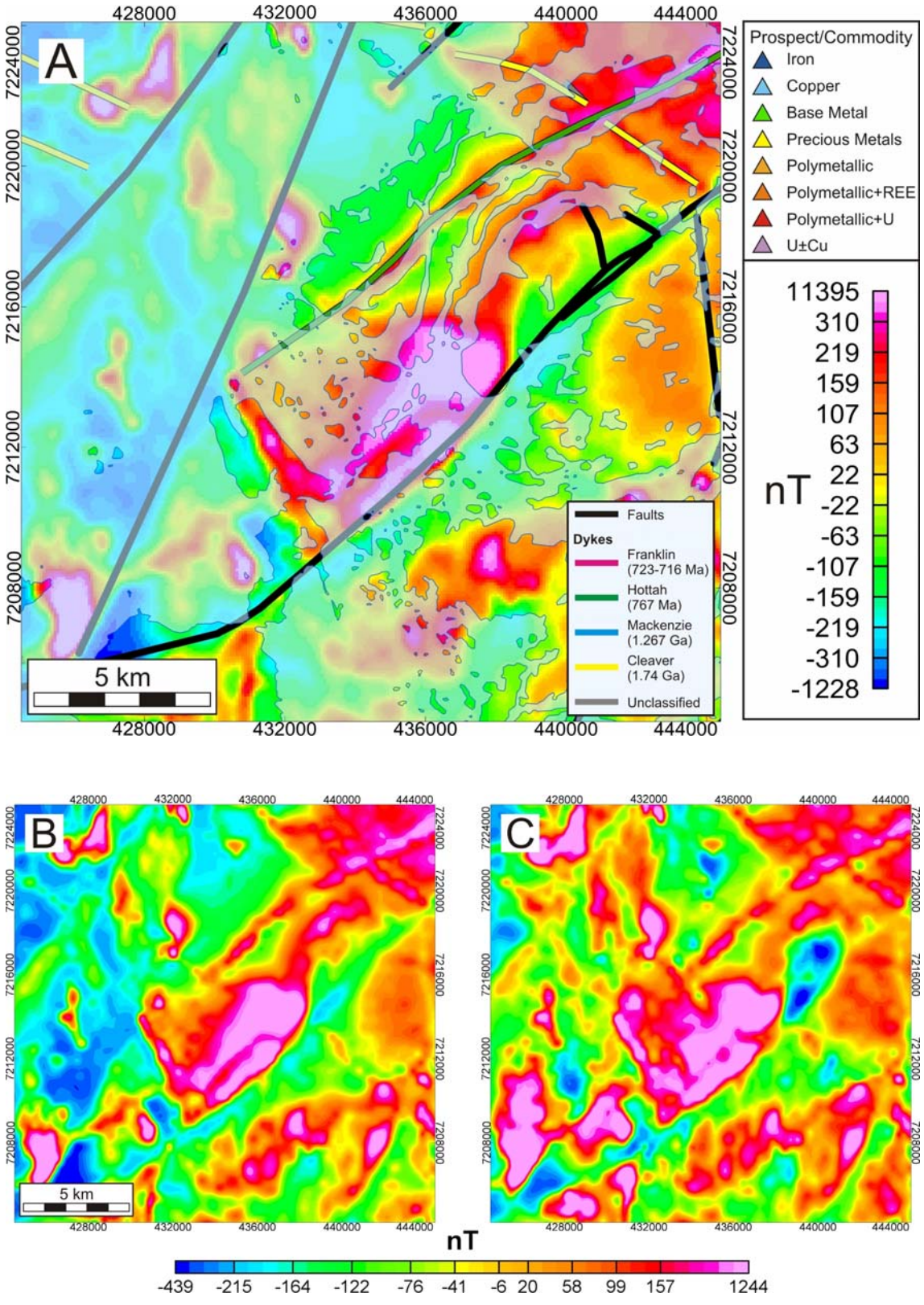

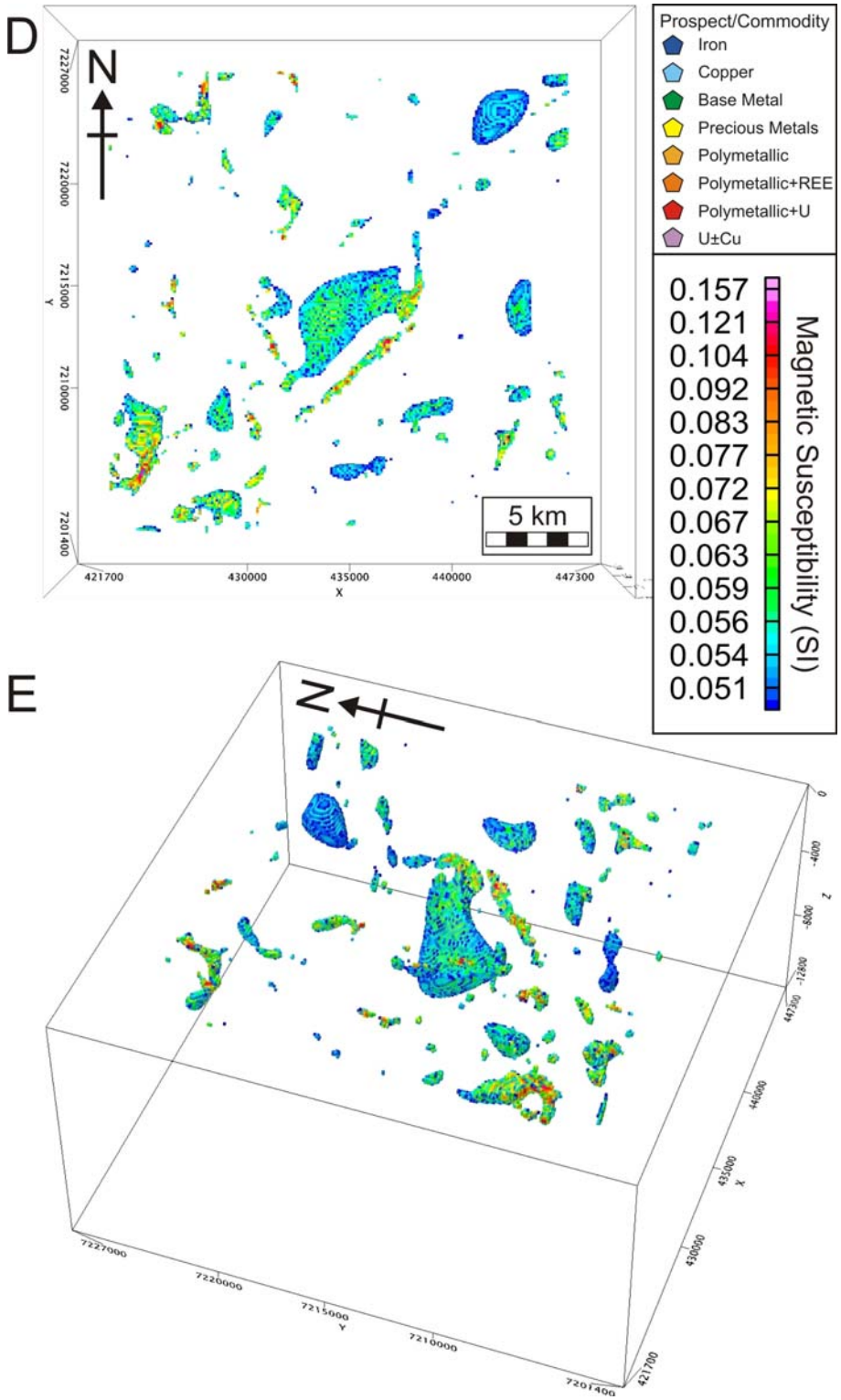

Figure 9: Model 7 – East Hottah area (see Table 2 and Fig. 2 for model location and parameters). a) Interpretation of aeromagnetic data (colour scale as in regional map, Fig. 2). Coloured lines show dykes. Black lines show faults. Coloured triangles show mineral prospects. b) Observed residual total magnetic field. c) Calculated residual total magnetic field. d) Plan view of 3D magnetic inversion model (magnetic susceptibility window of 0.05 – 0.15 SI). e) Perspective view of 3D magnetic inversion model. Coloured pentagons show mineral prospects.

Model 8 – Ham

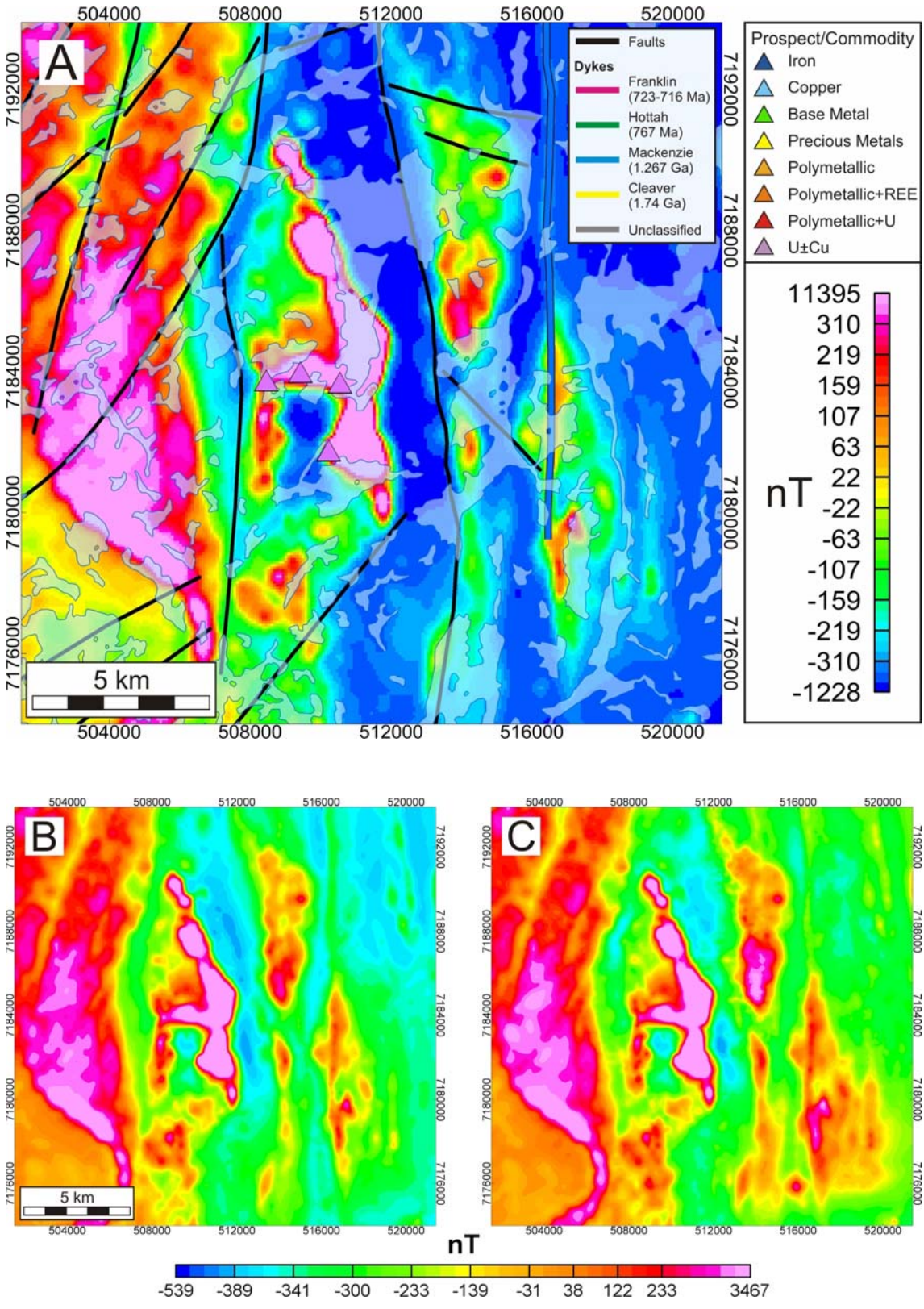
A
B
C
504000
508000
512000
516000
520000
7192000
7188000
7184000
7180000
7176000
Faults
Dykes
Franklin (723-716 Ma)
Hottah (767 Ma)
Mackenzie (1.267 Ga)
Cleaver (1.74 Ga)
Unclassified
Prospect/Commodity
Iron
Copper
Base Metal
Precious Metals
Polymetallic
Polymetallic+REE
Polymetallic+U
U±Cu
11395
310
219
159
107
63
22
-22
-63
-107
-159
-219
-310
-1228
nT
5 km
nT
-539
-389
-341
-300
-233
-139
-31
38
122
233
3467

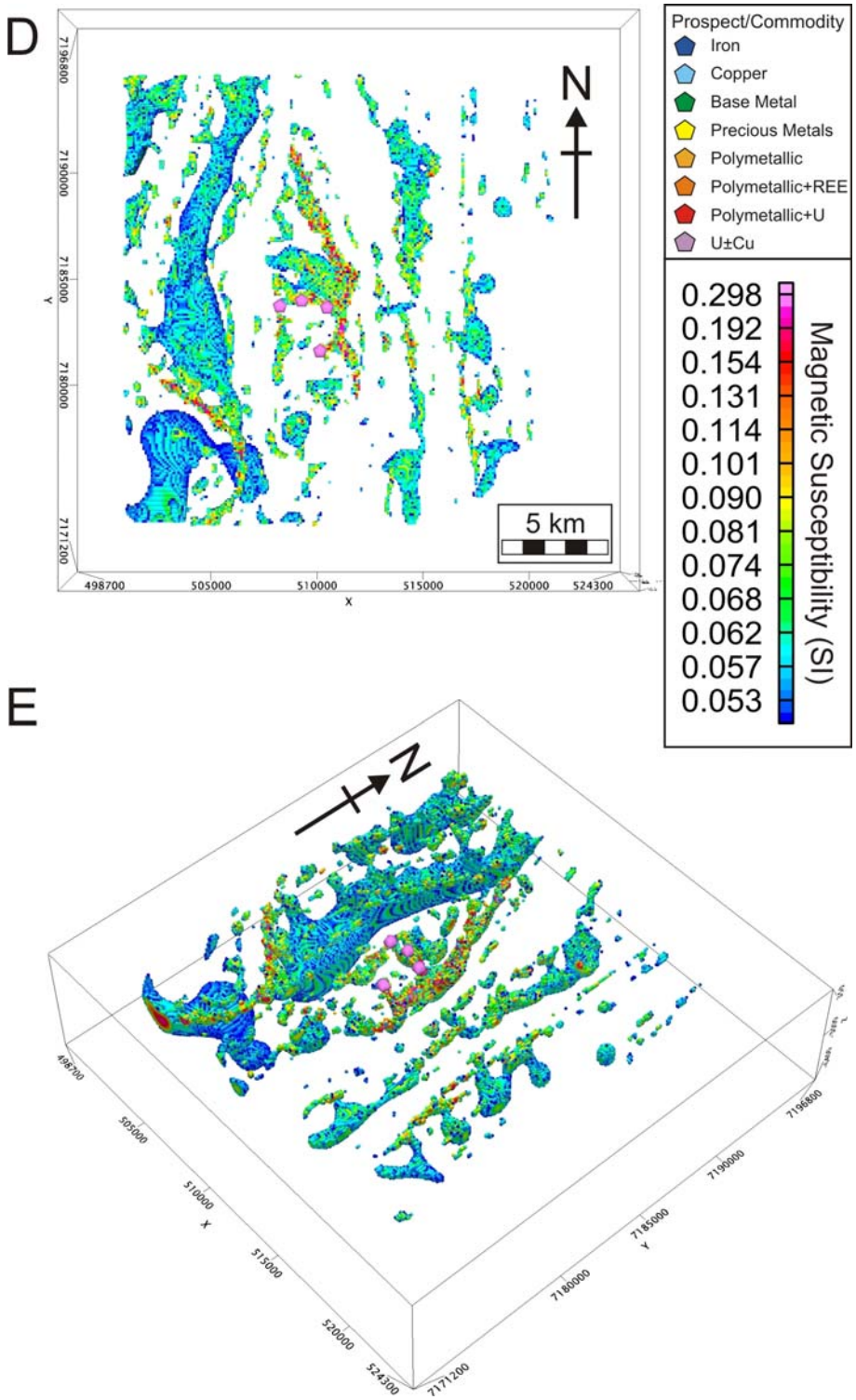

Figure 10: Model 8 - Ham area (see Table 2 and Fig. 2 for model location and parameters). a) Interpretation of aeromagnetic data (colour scale as in regional map, Fig. 2). Coloured lines show dykes. Black lines show faults. Coloured triangles show mineral prospects. b) Observed residual total magnetic field. c) Calculated residual total magnetic field. d) Plan view of 3D magnetic inversion model (magnetic susceptibility window of 0.05 – 0.2 SI). e) Perspective view of 3D magnetic inversion model. Coloured pentagons show mineral prospects.

Model 9 – JLD

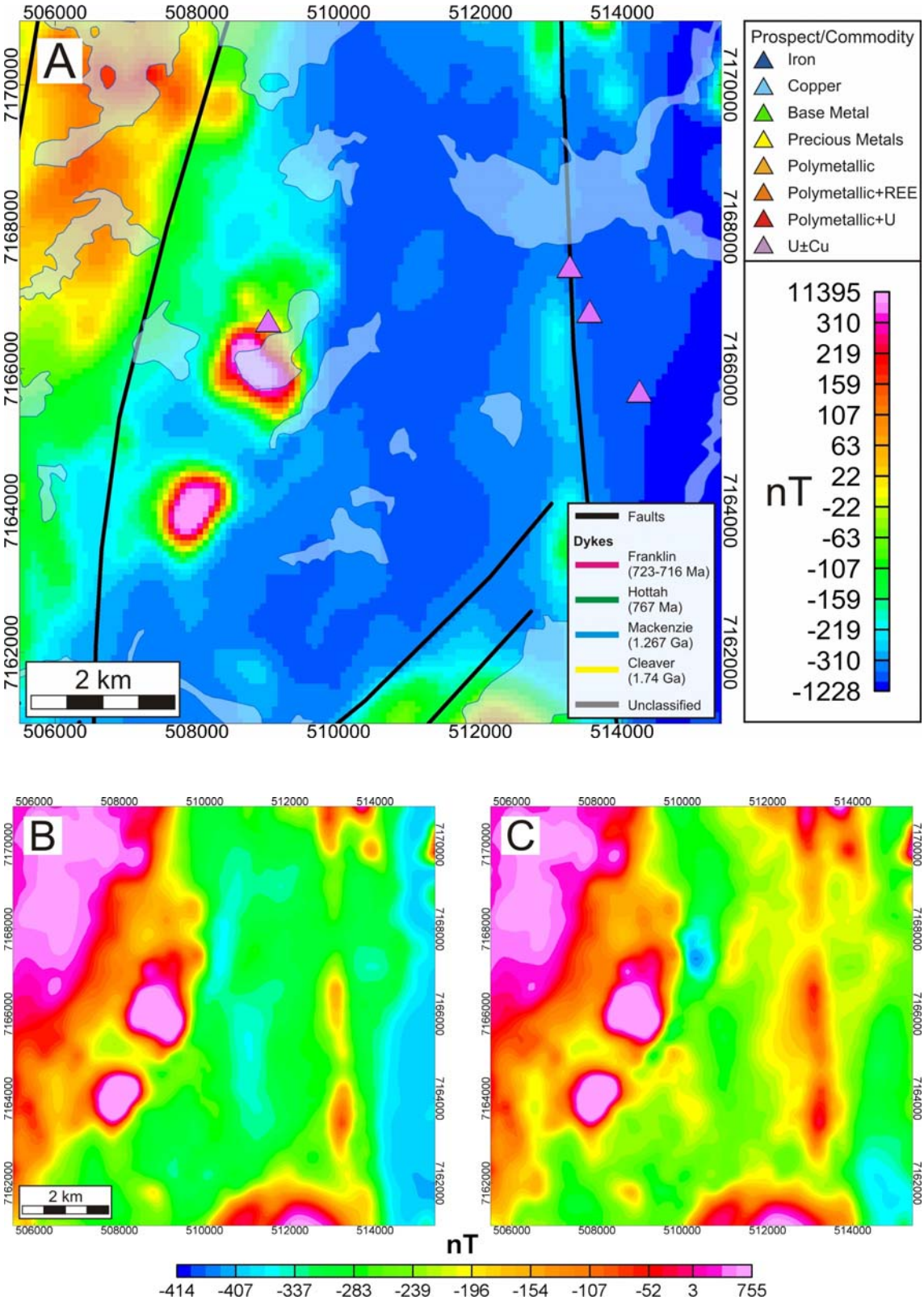
A
B
C
506000
508000
510000
512000
514000
7170000
7168000
7166000
7164000
7162000
Prospect/Commodity
Iron
Copper
Base Metal
Precious Metals
Polymetallic
Polymetallic+REE
Polymetallic+U
U±Cu
11395
310
219
159
107
63
22
-22
-63
-107
-159
-219
-310
-1228
nT
Faults
Dykes
Franklin (723-716 Ma)
Hottah (767 Ma)
Mackenzie (1.267 Ga)
Cleaver (1.74 Ga)
Unclassified
2 km
nT
-414
-407
-337
-283
-239
-196
-154
-107
-52
3
755

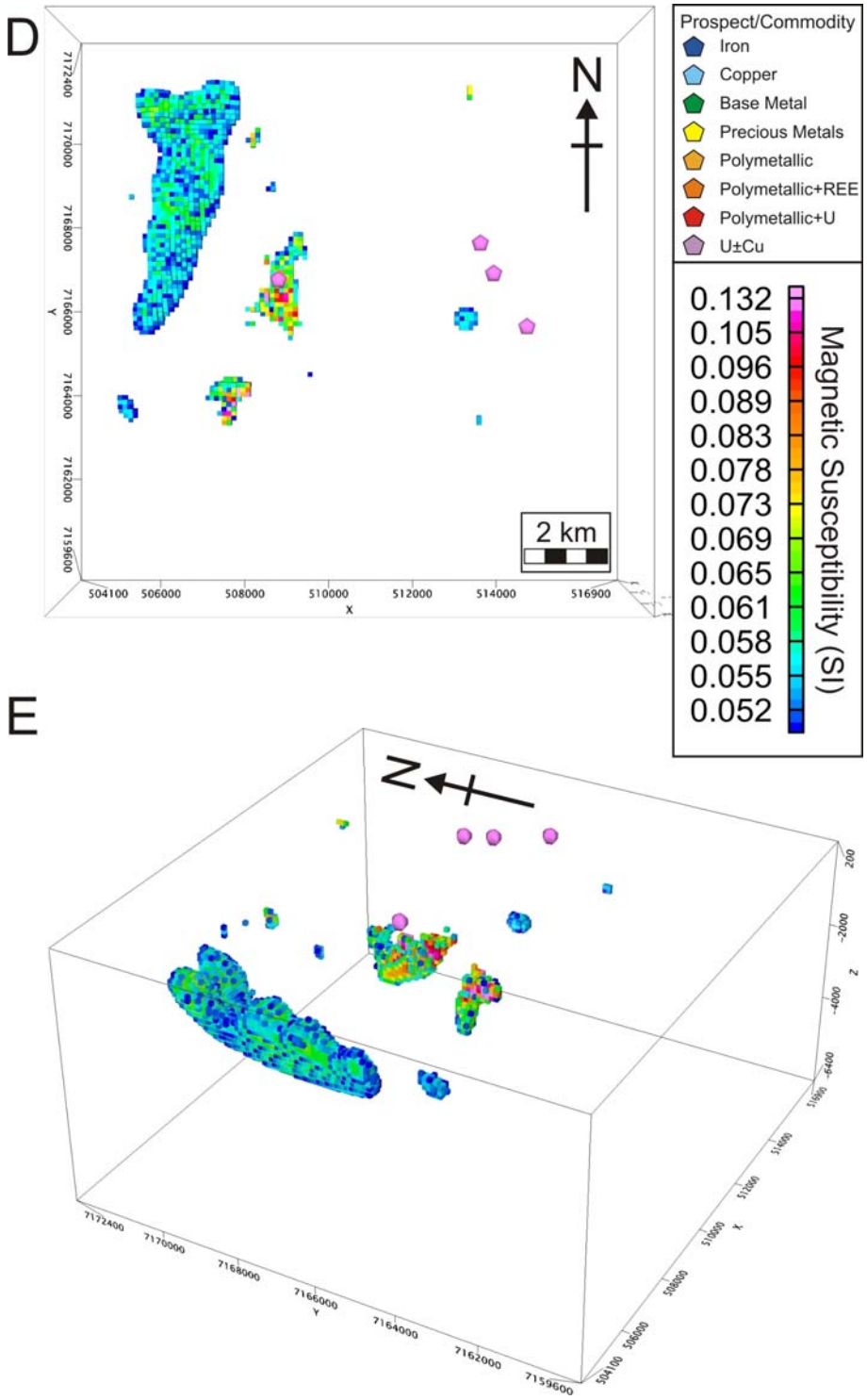

Figure 11: Model 9 - JLD area (see Table 2 and Fig. 2 for model location and parameters). a) Interpretation of aeromagnetic data (colour scale as in regional map, Fig. 2). Black lines show faults. Coloured triangles show mineral prospects. b) Observed residual total magnetic field. c) Calculated residual total magnetic field. d) Plan view of 3D magnetic inversion model (magnetic susceptibility window of 0.05 – 0.15 SI). e) Perspective view of 3D magnetic inversion model. Coloured pentagons show mineral prospects.

Model 10 – De Vries Lake

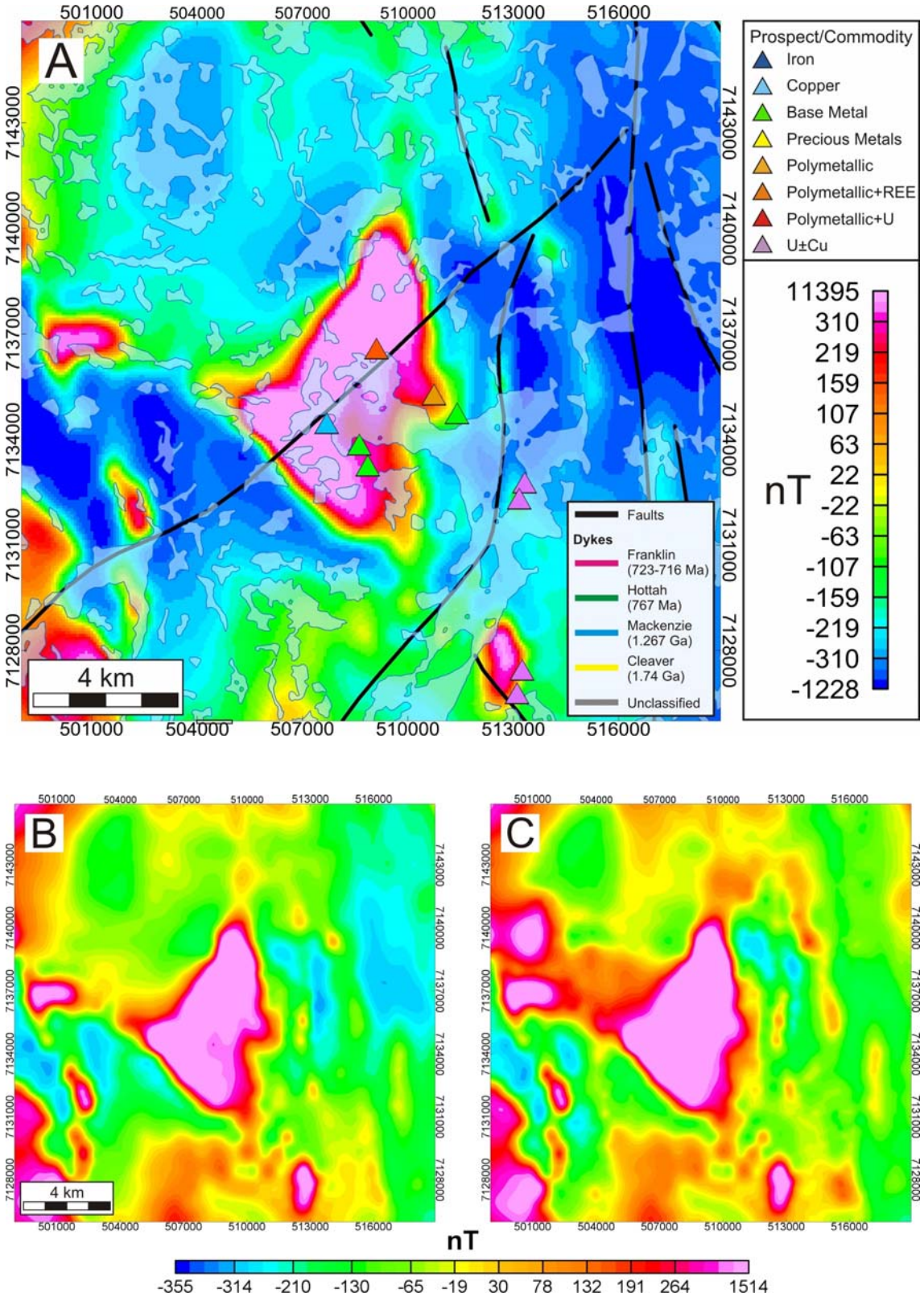

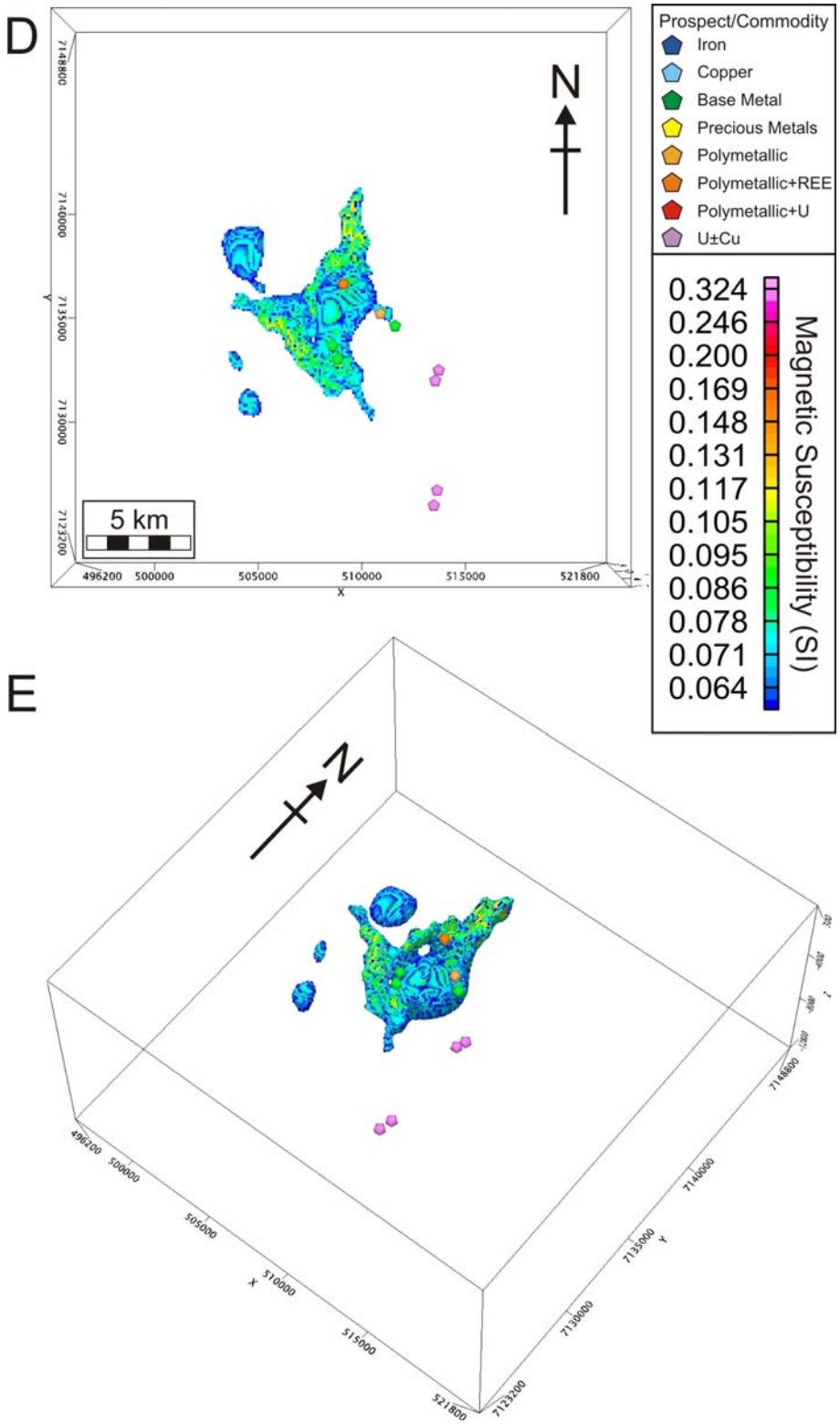

Figure 12: Model 10 - DeVries Lake area (see Table 2 and Fig. 2 for model location and parameters). a) Interpretation of aeromagnetic data (colour scale as in regional map, Fig. 2). Black lines show faults. Coloured triangles show mineral prospects. b) Observed residual total magnetic field. c) Calculated residual total magnetic field. d) Plan view of 3D magnetic inversion model (magnetic susceptibility window of 0.06 – 0.15 SI). e) Perspective view of 3D magnetic inversion model. Coloured pentagons show mineral prospects.

Model 11 – Fab Lake

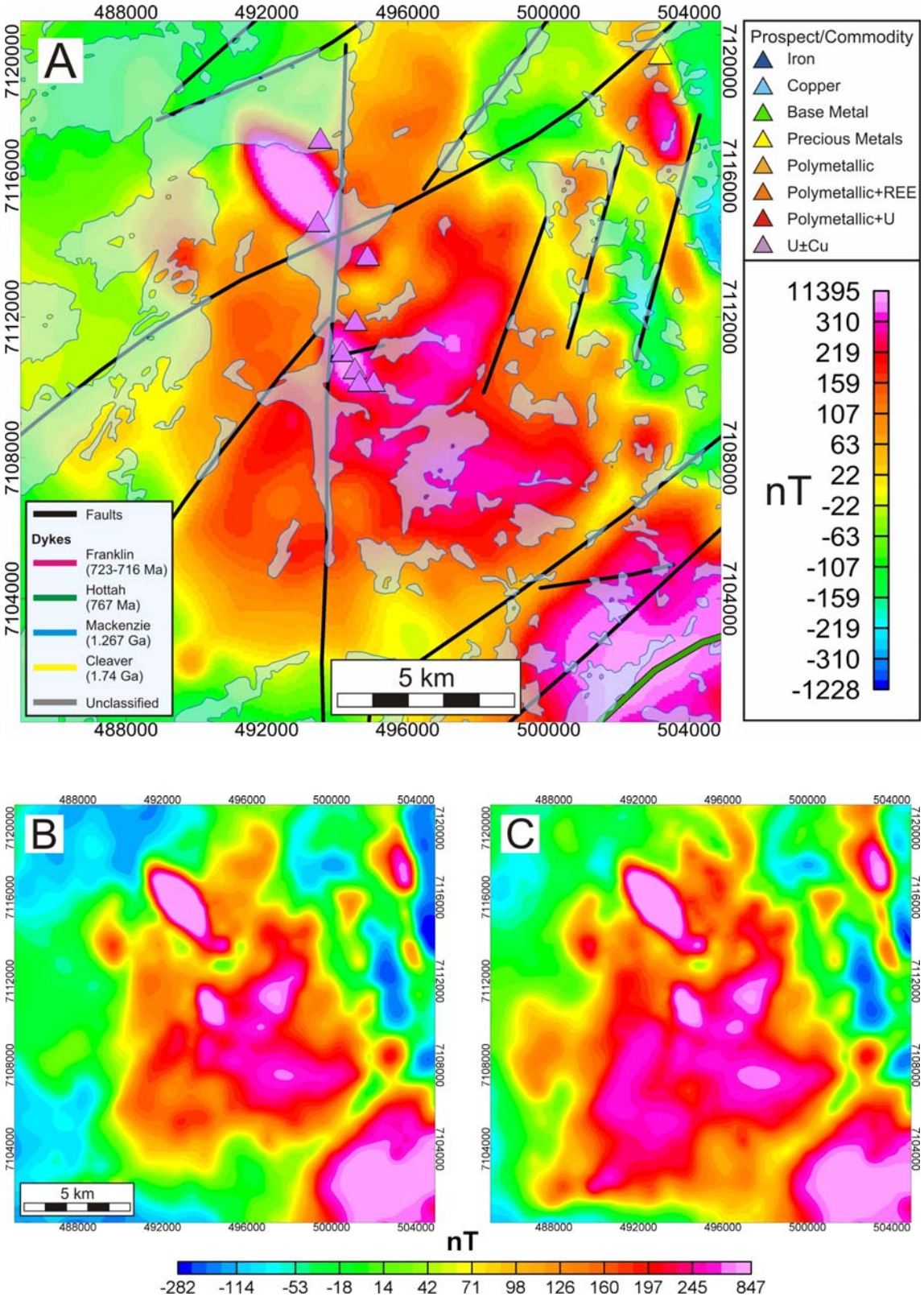

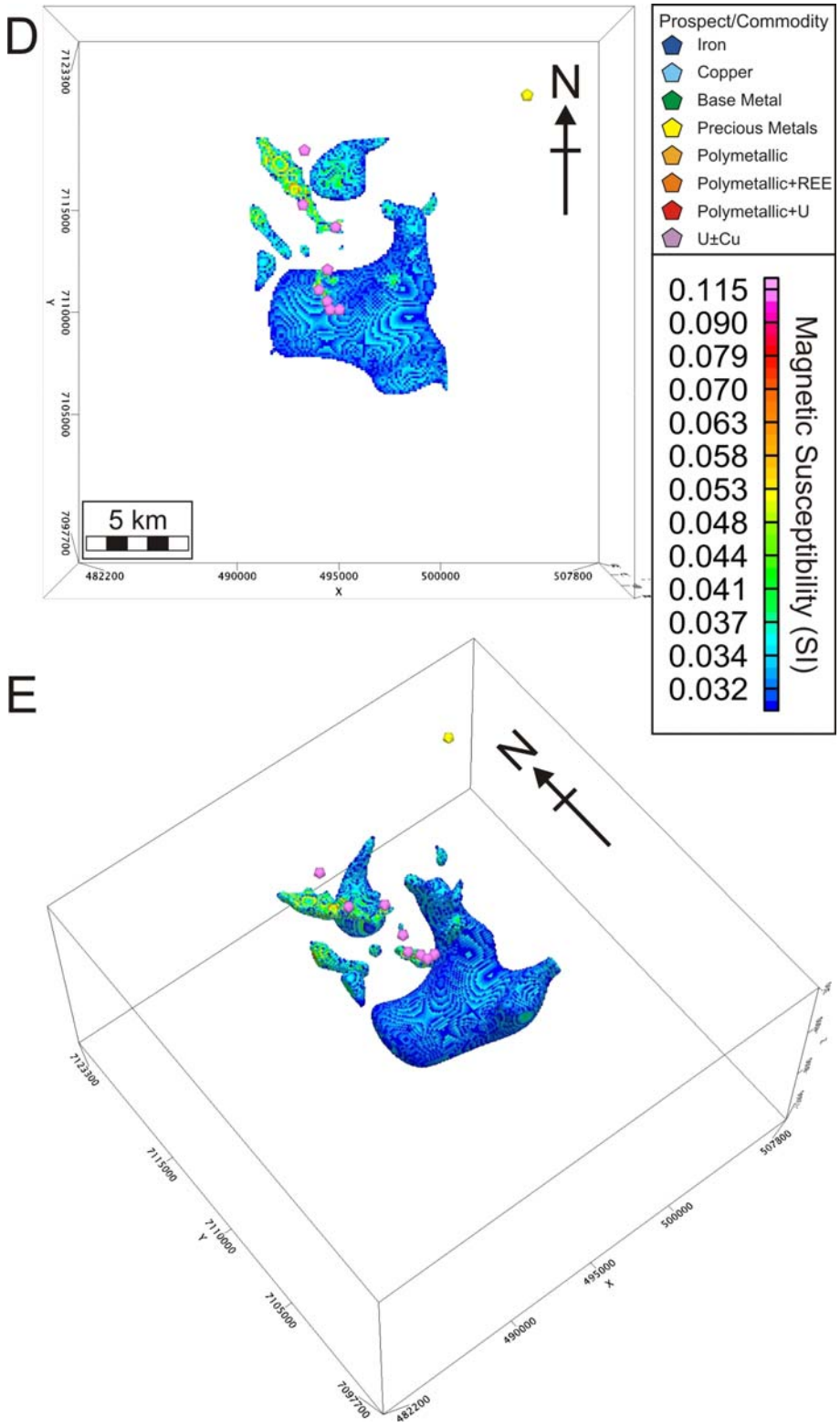

Figure 13: Model 11 - Fab Lake area (see Table 2 and Fig. 2 for model location and parameters). a) Interpretation of aeromagnetic data (colour scale as in regional map, Fig. 2). Coloured lines show dykes. Black lines show faults. Coloured triangles show mineral prospects. b) Observed residual total magnetic field. c) Calculated residual total magnetic field. d) Plan view of 3D magnetic inversion model (magnetic susceptibility window of 0.03 – 0.1 SI). e) Perspective view of 3D magnetic inversion model. Coloured pentagons show mineral prospects.

Model 12 – Cole Lake

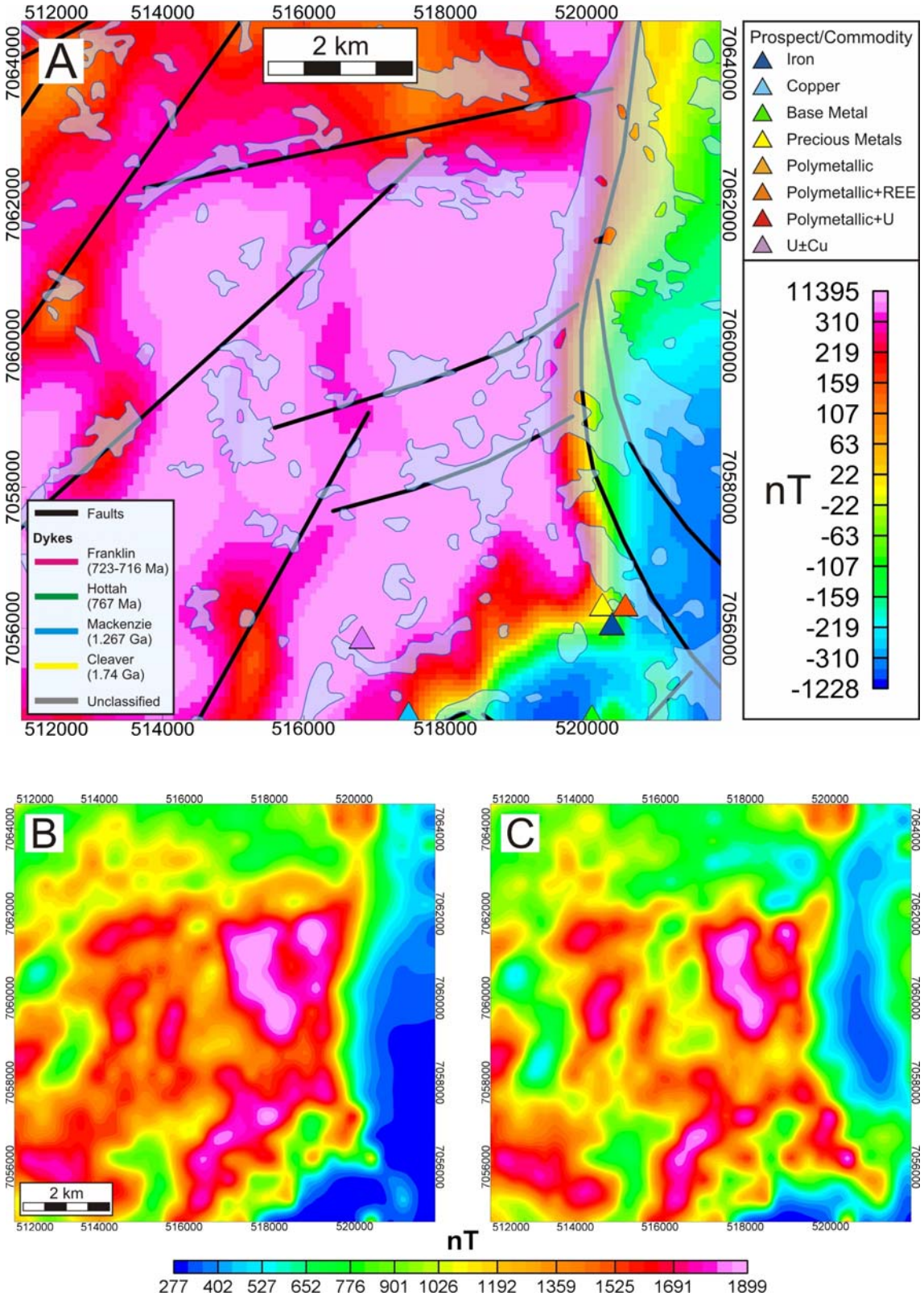

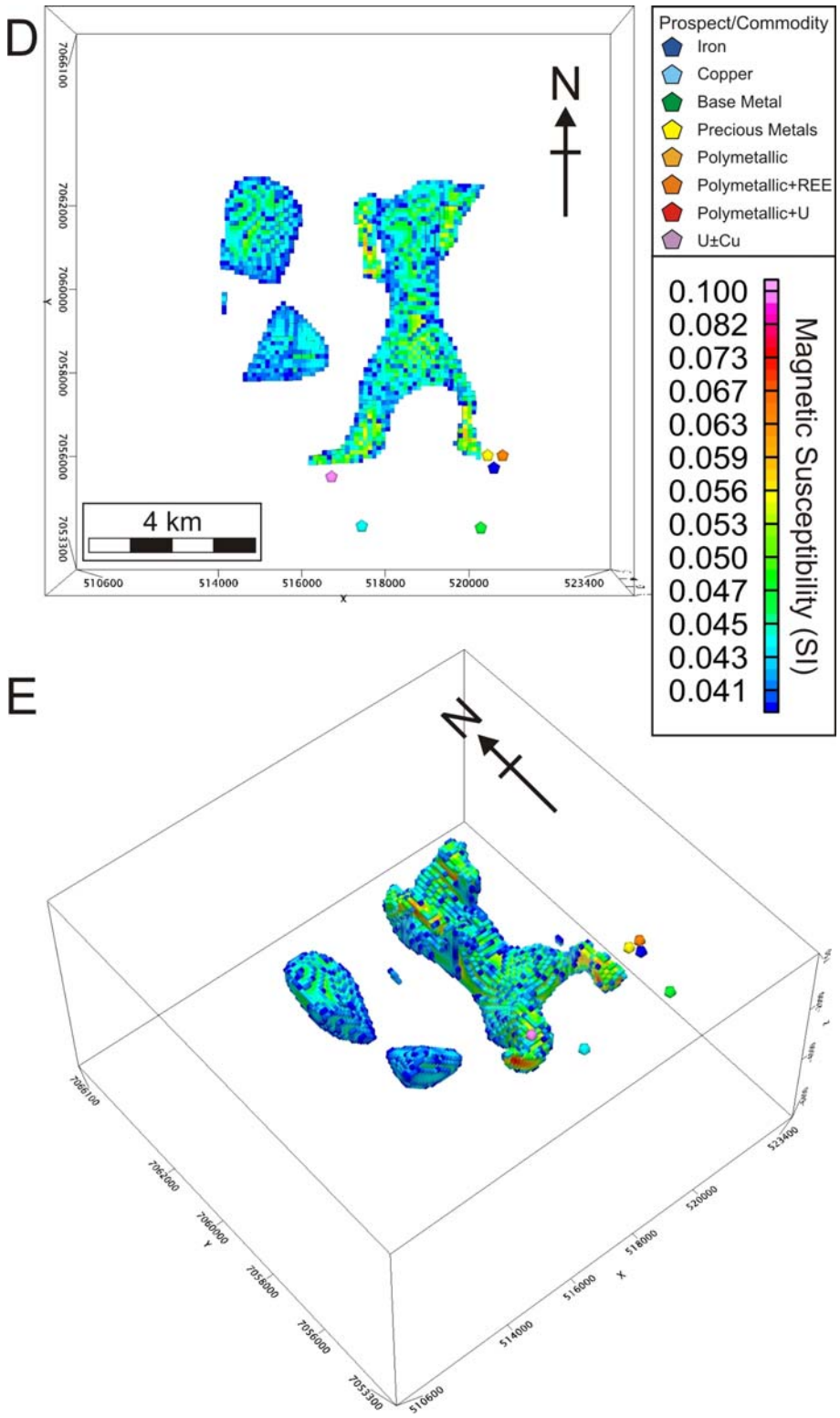

Figure 14: Model 12 - Cole Lake area (see Table 2 and Fig. 2 for model location and parameters). a) Interpretation of aeromagnetic data (colour scale as in regional map, Fig. 2). Black lines show faults. Coloured triangles show mineral prospects. b) Observed residual total magnetic field. c) Calculated residual total magnetic field. d) Plan view of 3D magnetic inversion model (magnetic susceptibility window of 0.04 – 0.24 SI). e) Perspective view of 3D magnetic inversion model. Coloured pentagons show mineral prospects.

Model 13– NICO

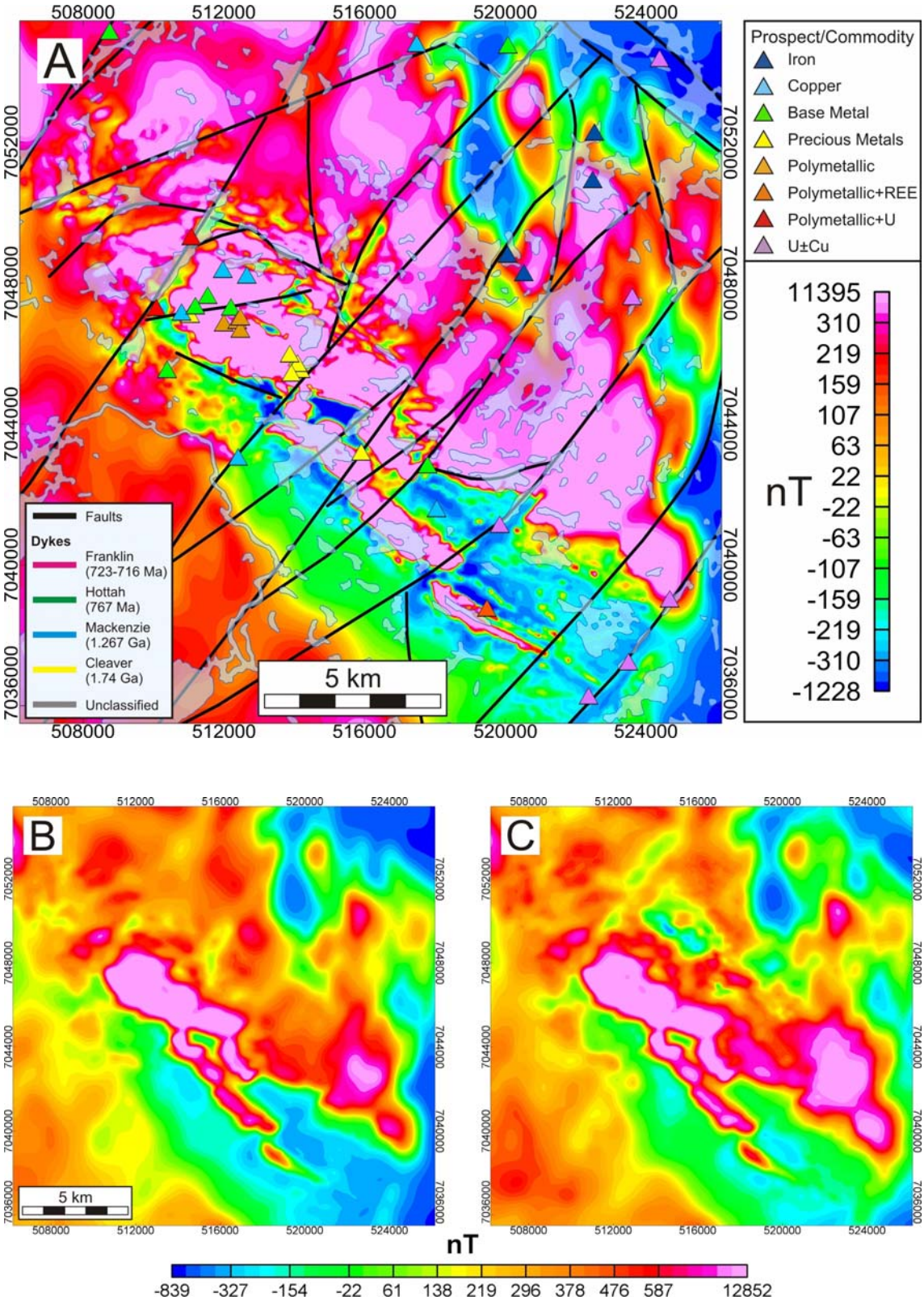

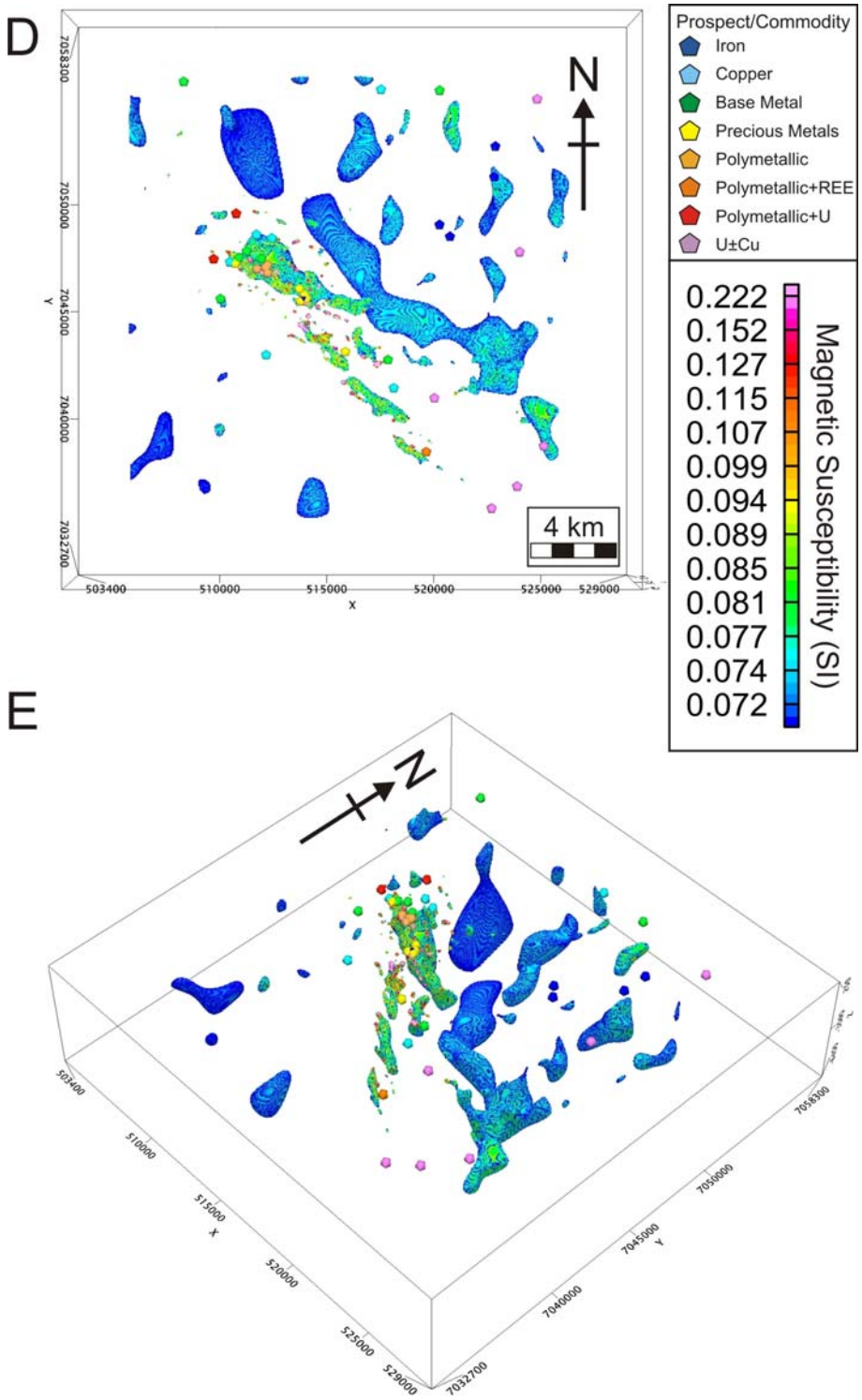

Figure 15: Model 13 - NICO area (see Table 2 and Fig. 2 for model location and parameters). a) Interpretation of aeromagnetic data (colour scale as in regional map, Fig. 2). Black lines show faults. Coloured triangles show mineral prospects. b) Observed residual total magnetic field. c) Calculated residual total magnetic field. d) Plan view of 3D magnetic inversion model (magnetic susceptibility window of 0.07 – 0.5 SI). e) Perspective view of 3D magnetic inversion model. Coloured pentagons show mineral prospects.

Acknowledgements

The research is part of the Geomapping for Energy and Mineral Program of Natural Resources Canada and was conducted in collaboration with the Northwest Territories Geoscience Office South Wopmay Bedrock Mapping project (Strategic Investments in Northern Economic Development program, Indian and Northern Affairs Canada). Fieldwork was permitted under Aurora Research Institute Research Licenses 14844, 14639 and 14548, Wek'èezhìi Land and Water Board Land Use Permits Class A W2010J0004 and W2009C0001, NWT archaeological sites database agreements DR2010-390 and DR2009-335 and Polar Continental Shelf Program projects 010009, 50709 and 00410. We wish to thank Bruce Kienlen, Diamond's North Resources Ltd. and Robin Goad, Fortune Minerals Ltd. for providing high-resolution geophysical data. We also thank all field participants of the IOCG-Great Bear project and reviewers L. Corriveau and M. Pilkington.

References

Belperio, A., 2007. Prominent Hill: A hematite-dominated, iron oxide copper-gold system. Economic Geology 102, 1499–1510.

Bleeker, W., and LeCheminant, A.N., 2007. The 'Dessert Lake' red-bed basin; a newly recognized Proterozoic Basin (outlier) overlying the southern extension of the Slave and Bear Provinces. Geological Association of Canada, Mineralogical Association of Canada; joint annual meeting, Yellowknife, NT, Canada, 32, 8-9.

Bowring, S.A., 1984. U-Pb zircon geochronology of early Proterozoic Wopmay Orogen, N.W.T. Canada; an example of rapid crustal evolution. Ph.D. Thesis, University of Kansas.

Cook, F.A., van der Veldon, A.J., Hall, K.W., and Roberts, B.J., 1999. Frozen subduction in Canada's Northwest Territories: Lithoprobe deep lithospheric profiling on the western Canadian Shield. Tectonics 18, 1–24.

Buchan, K.L., and Ernst, R.E., 2004. Diabase dyke swarms and related units in Canada and adjacent regions. Geological Survey of Canada, "A" Series Map 2022A; 39 pages (1 sheet) 1 CD-ROM.

Buchan, K.L., Ernst, R.E., Bleeker, W., Davis, W.J., Villeneuve, M., van Breemen, O., Hamilton, M.A., and Söderlund, U., 2010. Proterozoic magmatic events of the Slave Craton, Wopmay Orogen and environs. Geological Survey of Canada, Open File 5985; Poster and CD-ROM.

Cooper Minerals, 2007. The Great Bear Lake iron oxide-copper-gold district of Northwest Territories, Canada. Presentation (http.//www.cooperminerals.com/frame.php?url=pdf%2FProperties-GREAT%2520BEAR%2520LAKE%2C%2520CANADA-2007-08-18.pdf).

Corriveau, L., Mumin, A.H., and Setterfield, T., 2010a. IOCG environments in Canada: Characteristics, geological vectors to ore and challenges, in: Porter, T.M. (Ed.), Hydrothermal iron oxide copper-gold and related deposits: A global perspective, volume 4-advances in the understanding of IOCG deposits. Porter Geoscience Consultancy Publishing, Adelaide, pp. 311–344.

Corriveau, L., Williams, P.J., and Mumin, A.H., 2010b. Alteration vectors to IOCG mineralization – from uncharted terranes to deposits, in: Corriveau, L., Mumin, A.H. (Eds.), Exploring for iron oxide

copper-gold deposits: Canada and global analogues. Geological Association of Canada Short Course Notes, 20, pp. 89–110.

Davis, W., Corriveau, L., van Breemen, O., Bleeker, W., Montreuil, J-F., Potter, E., and Pelleter, E., 2011. Timing of IOCG mineralizing and alteration events within the Great Bear magmatic zone, in: Fischer, B.J., Watson, D.M., (Compilers), 39th Annual Yellowknife Geoscience Forum Abstracts. Northwest Territories Geoscience Office, Yellowknife, NT, YKGSF Abstracts Volume 2011, pp. 33.

Gandhi, S.S., Mortensen, J.K., Prasad, N., and van Breemen, O., 2001. Magmatic evolution of the southern Great Bear continental arc, northwestern Canadian Shield: Geochronological constraints. Canadian Journal of Earth Sciences 38, 767–785.

Goad, R.E., Mumin, A.H., Duke, N.A., Neale, K.L., and Mulligan, D.L., 2000a. Geology of the Proterozoic iron oxide-hosted, NICO cobalt-gold-bismuth, and Sue Dianne copper-silver deposits, southern Great Bear magmatic zone, Northwest Territories, Canada, in: Porter, T.M., (Ed.), Hydrothermal iron oxide copper-gold and related deposits. A global perspective, volume 1. Porter Geoscience Consultancy Publishing, Adelaide, pp. 249–267.

Goad, R.E., Mumin, A.H., Duke, N.A., Neale, K.L., Mulligan, D.L., and Camier, W.J., 2000b. The NICO and Sue-Dianne Proterozoic, iron oxide-hosted, polymetallic deposits, Northwest Territories. Application of the Olympic Dam model in exploration. Exploration Mining Geology 9, 123–140.

Groves, D.I., Bierlein, F.P., Meinert, L.D., and Hitzman, M.W., 2010. Iron oxide copper-gold (IOCG) deposits through Earth history. Implications for origin, lithospheric setting, and distinction from other epigenetic iron oxide deposits. Economic Geology 105, 641–654.

Harvey, B.J.A., Kiss, F., and Carson, J.M., 2009. Geophysical series, NTS 86 F, parts of 86 E, 86 G, 86 J, 86 K and 86 L, airborne geophysical survey of the northern Great Bear Magmatic Zone, Northwest Territories. Geological Survey of Canada, Open Files 6289 to 6299 and Northwest Territories Geoscience Office, NWT Open File 2009-05; 10 sheets.

Hayward, N., Enkin, R.J., Corriveau, L., Montreuil, J-F., and Kerswill, J., 2013. The application of rapid potential field methods for the targeting of IOCG mineralisation based on physical property data, Great Bear magmatic zone, Canada. Journal of Applied Geophysics, 94, 42–58.

Hayward, N., and Oneschuk, D., 2011. Geophysical series, regional geophysical compilation project, Great Bear Magmatic Zone, Northwest Territories and Nunavut, NTS 85 M and N, and 86 C, D, E, F, K and L. Geological Survey of Canada, Open File, 6835/NTGO Open File 2011-05.

Hetu, R.J., Holman, P.B., Charbonneau, B.W., Prasad, N., and Gandhi, S.S., 1994. Airborne geophysical survey, Mazenod Lake, NWT, 1994. Geological Survey of Canada, Open File 2806.

Hildebrand, R.S., 1986. Kiruna-type deposits; their origin and relationship to intermediate subvolcanic plutons in the Great Bear magmatic zone, Northwest Canada. Economic Geology 81, 640–659.

Hildebrand, R.S., 2011. Geologic synthesis, northern Wopmay orogen/Coppermine homocline; Geological Survey of Canada Open File Map 6390 (1:500 000 scale).

Hildebrand, R.S., Hoffman, P.F., and Bowring, S.A., 1987. Tectono-magmatic evolution of the 1.9-Ga Great Bear magmatic zone, Wopmay Orogen, Northwestern Canada. Journal of Volcanology and Geothermal Research 32, 99–118.

Hildebrand, R.S., Hoffman, P.F., and Bowring, S.A., 2010a. The Calderian orogeny in Wopmay orogen (1.9 Ga), northwestern Canadian Shield. Geological Society of America Bulletin 122, 794–814.

Hildebrand, R.S., Hoffman, P.F., Housh, T., and Bowring, S.A., 2010b. The nature of volcano-plutonic relations and the shapes of epizonal plutons of continental arcs as revealed in the Great Bear magmatic zone, northwestern Canada. Geosphere 6, 1–28.

Hitzman, M.C., 2000. Iron oxide-Cu-Au deposits. What, where, when, and why?, in: Porter, T.M., (Ed.), Hydrothermal iron oxide copper-gold and related deposits. A global perspective, volume 1. Porter Geoscience Consultancy Publishing, Adelaide, pp. 9–25.

Hitzman, M.W., and Valenta, R.K., 2005. Uranium in iron oxide-copper-gold (IOCG) systems. Economic Geology 100, 1657–1661.

Hitzman, M.C., Oreskes, N., and Einaudi, M.T., 1992. Geological characteristics and tectonic setting of Proterozoic iron oxide (Cu-U-Au-REE) deposits. Precambrian Research 58, 241–287.

Hoffman, P.F., 1980. Wopmay Orogen. A Wilson cycle of Early Proterozoic age in the northwest of the Canadian Shield, in: Strangway, D.W., (Ed.), The continental crust and its mineral deposits. Geological Association of Canada, Special Paper 20, pp. 523–549.

Hoffman, P.F., and Bowring, S.A., 1984. Short-lived 1.9 Ga continental margin and its destruction, Wopmay Orogen, northwest Canada. Geology 12, 68–72.

Hoffman, P., and Hall, L., 1993. Geology, Slave craton and environs, District of Mackenzie, Northwest Territories. Geological Survey of Canada, Open File 2559; 1 sheet 1 CD-ROM.

Hoffman, P.F., and McGlynn, J., 1977. Great Bear batholith. A volcano-plutonic depression, in: Baragar, W.R.A., Coleman, L.C., Hall, J.M., (Eds.), Volcanic regimes in Canada. Geological Association of Canada, Special Paper 16, pp. 169–192.

Irving, E., Baker, J., Hamilton, M., and Wynne, P.J., 2004. Early Proterozoic geomagnetic field in western Laurentia: Implications for paleolatitudes, local rotations and stratigraphy. Precambrian Research 129, 251–270.

Jackson, V.A., 2008. Preliminary geologic map of part of the Southern Wopmay Orogen (parts of NTS 86B and 86C; 2007 updates); map with descriptive notes. NWT Open Report 2008-007.

Jébrak, M., 2010. Use of breccias in IOCG(U) exploration, in: Corriveau, L., Mumin, A.H., (Eds.), Exploring for iron oxide copper-gold deposits: Canada and global analogues. Geological Association of Canada, Short Course Notes 20, pp. 79–88.

Kiss, F., and Coyle, M., 2011. Hottah Lake aeromagnetic survey, Northwest Territories, parts of NTS 86 C/5, 12, 86 D/5, 6, 7, 8, 9, 10, 11, 12. NWT Open File 2011-03; Geological Survey of Canada, Open Files 6851 to 6854.

Montreuil, J.-F., Corriveau, L., and Grunsky, E.C., 2013. Compositional data analysis of IOCG systems, Great Bear magmatic zone, Canada: To each alteration types its own geochemical signature. Geochemistry: Environment, Exploration, Analysis, in press.

Mumin, A.H., Corriveau, L., Somarin, A.K., and Ootes, L., 2007. Iron oxide copper-gold-type polymetallic mineralization in the Contact Lake Belt, Great Bear Magmatic Zone, Northwest Territories, Canada. Exploration and Mining Geology 16, 187–208.

Mumin, A.H., Somarin, A.K., Jones, B., Corriveau, L., Ootes, L., and Camier, J., 2010. The IOCG-porphyry-epithermal continuum of deposits types in the Great Bear magmatic zone, Northwest Territories, Canada, in: Corriveau, L., Mumin, A.H., (Eds.), Exploring for iron oxide copper-gold deposits: Canada and global analogues. Geological Association of Canada, Short Course Notes 20, pp. 59–78.

NTGO, 2006. Aeromagnetic Survey, Lac la Martre Area, Northwest Territories, parts of 85N, 85M, 86C, 86D. Northwest Territories Geoscience Office (NTGO), NWT Open File 2006-004, 8 maps and digital data.

NTGO, 2008. Airborne magnetic and gamma-ray spectrometric survey of the Southwestern Wopmay Orogen, Northwest Territories, parts of NTS 86 C, 86 E and 86 F, block A (parts of NTS 86 C/7, 86 C/9 and 86 C/10). NWT Open File 2008-02. Geological Survey of Canada, Open File 5821; 10 sheets.

NTGO, 2012. NORMIN – The Northern Minerals Database. NWT Geoscience Office. http://www.nwtgeoscience.ca/normin/

Oliver, N.H.S., Butera, K.M., Rubenach, M.J., Marshall, L.J., Cleverley, J.S., Mark, G., Tullemans, F., and Esser, D., 2008. The protracted hydrothermal evolution of the Mount Isa Eastern Succession: A review and tectonic implications. Precambrian Research 163, 108–130.

Pilkington, M., 2009. 3D magnetic data-space inversion with sparseness constraints. Geophysics, 74, L7–L15.

Porter, T.M., 2010a. Current understanding of iron oxide associated-alkali altered mineralised systems. Part 1 - An overview, in: Porter, T.M., (Ed.), Hydrothermal iron oxide copper-gold and related deposits. A global perspective, volume 3, Advances in the understanding of IOCG deposits. Porter Geoscience Consultancy Publishing, Adelaide, pp. 5–32.

Porter, T.M., 2010b. The Carrapateena iron oxide copper gold deposit, Gawler craton, South Australia: A review, in: Porter, T.M., (Ed.), Hydrothermal iron oxide copper-gold and related deposits. A global perspective, volume 3, Advances in the understanding of IOCG deposits. Porter Geoscience Consultancy Publishing, Adelaide, pp. 191-200.

Pritchard, R.A., 1995. Dighem survey for Fortune Minerals Limited NICO/Olympic Dam properties, N.W.T. NTS 85N/7, 10, 15. Report 1222-B.

Sandrin, A., Berggren, R., and Elming, S.-Å., 2007. Geophysical targeting of Fe-oxide Cu-(Au) deposits west of Kiruna, Sweden. Journal of Applied Geophysics 61, 92–101.

Sandrin, A., Eldfelt, Å., Waight, T.E., Berggren, R., and Elming, S.-Å., 2009. Physical properties and petrologic description of rock samples from an IOCG mineralized area in the northern Fennoscandian Shield, Sweden. Journal of Geochemical Exploration 103, 80–96.

Skirrow, R., 2010. "Hematite-group" IOCG±U ore systems. Tectonic settings, hydrothermal characteristics, and Cu-Au and U mineralizing processes, in: Corriveau, L., Mumin, A.H., (Eds.), Exploring for iron oxide copper-gold deposits: Canada and global analogues. Geological Association of Canada, Short Course Notes 20, pp. 39–58.

Smith, R.J., 2002. Geophysics of iron oxide copper-gold deposits, in: Porter, T.M., (Ed.), Hydrothermal Iron Oxide Copper Gold and related deposits. A global perspective, volume 2. Porter Geoscience Consultancy Publishing, Adelaide, pp. 357–367.

Tirrul, R., 1984. Regional pure shear deformation by conjugate transcurrent faulting, externides of Wopmay Orogen, N. W. T. Geological Association of Canada-Mineralogical Association of Canada, Program with Abstracts 9, pp. 111.

Webb, M., and Rowston, P., 1995. The geophysics of the Ernest Henry Cu-Au deposit (N.W.) Qld. Exploration Geophysics 26, 51–59.

Williams, P.J., 2010a. Classifying IOCG deposits, in: Corriveau, L., Mumin, A.H., (Eds.), Exploring for iron oxide copper-gold deposits: Canada and global analogues. Geological Association of Canada, Short Course Notes 20, pp. 13–22.

Williams, P.J., 2010b. "Magnetite-group" IOCGs with special reference to Cloncurry (NW Queensland) and Northern Sweden. Settings, alteration, deposit characteristics, fluid sources, and their relationship to apatite-rich iron ores, in: Corriveau, L., Mumin, A.H., (Eds.), Exploring for iron oxide copper-gold deposits: Canada and global analogues. Geological Association of Canada, Short Course Notes 20, pp. 23–38.

Williams, P.J., Barton, M.D., Johnson, D.A., Fontbote, L., de Haller, A., Mark, G., Oliver, N.H.S., and Marschik, R., 2005. Iron oxide copper-gold deposits; geology, space-time distribution, and possible modes of origin. Economic Geology 100th Anniversary Volume, pp. 371–406.